# Journal of Materials Chemistry A

Accepted Manuscript






ROYAL SOCIETY OF CHEMISTRY

www.rsc.org/materialsA

Journal of Materials Chemistry A

REVIEW

# Strategies succeed in improving the lithium-ion storage properties of silicon nanomaterials

Received 00th January 20xx,
Accepted 00th January 20xx

DOI: 10.1039/x0xx00000x

www.rsc.org/

Fei-Hu Du, Kai-Xue Wang* and Jie-Sheng Chen*

Silicon is of scientific and practical interest in lithium-ion batteries (LIBs) due to its natural abundance, low toxicity, moderate working potential, and high theoretical capacity. However, its huge volume variation during lithiation and delithiation processes leads to the pulverization of silicon particles and subsequently results in fast capacity fade of the electrodes. Furthermore, the intrinsic electric conductivity of Si is relatively low and lithium diffusion in Si is rather slow. These issues hinder the practical application of Si in LIBs. In the past decade, significant improvements in the anode's cycleability and rate capability have been achieved by the control of the nanostructure and morphology of Si electrode and incorporation of conductive species. In this review, the preparation methods and electrochemical performance of these Si electrode nanomaterials are summarised. The mechanisms behind the performance enhancement are illustrated. Moreover, factors that affect the performance of Si anodes, such as electrolyte additives, binders, and current collectors, are also discussed. We aim to shed some light on some emerging directions for future research on Si anodes in LIBs.

## 1. Introduction

The increasing depletion of non-renewable fossil fuels and the greenhouse gas emissions have aroused intense interest in exploring environmentally friendly energy resources (EERs).[1,2] However, most EERs, such as wind and solar energy, are intermittent, and hence highly efficient energy storage devices are required.[3] In this regard, lithium-ion batteries (LIBs) with relatively high energy and power densities can play a critically important role in the practical utilization of such EERs. LIBs have also been regarded as ideal power sources for electric vehicles (EVs) and hybrid electric vehicles (HEVs).[4] As a key component, electrode materials play an important role in the electrochemical performance of LIBs. Currently, graphite with theoretical capacity of only 372 mA h $g^{-1}$ is used as the anode material in commercial LIBs.[5] To satisfy the demand of EERs, EVs and HEVs for LIBs with high energy and power densities, considerable efforts have been devoted to alloy-type anodes with high theoretical capacity, including silicon,[5] phosphorus,[6-8] germanium,[9,10] and tin[11-16].

Among all alloy-type anodes, Si has large theoretical capacity (4200 mA h $g^{-1}$ by forming $Li_{22}Si_5$) and low discharge potential (~370 mV *vs.* $Li/Li^+$), leading to high energy density of batteries.[17] Si is the second-most abundant element in the

*School of Chemistry and Chemical Engineering, Shanghai Jiao Tong University, Shanghai 200240, P. R. China. E-mail: k.wang@sjtu.edu.cn; chemcj@sjtu.edu.cn; Fax: +86-21-54741297; Tel: +86-21-34201273*

*Fei-Hu Du received his BS degree (2008) and his MS degree (2011) in inorganic chemistry from Jiangsu University. He obtained his PhD degree in the School of Chemistry and Chemical Engineering at Shanghai Jiao Tong University in 2015. His research interest is primarily focused on inorganic materials, particularly on silicon-based electrode materials for Li ion batteries.*

*Prof. Kai-Xue Wang obtained his PhD degree in inorganic chemistry from Jilin University in 2002. He worked as a postdoctoral researcher at University College Cork, Ireland and then JSPS research fellow at National Institute of Advanced Industrial Science and Technology, Japan from 2003 to 2009. Since 2009, he has been a professor in the School of Chemistry and Chemical Engineering, Shanghai Jiao Tong University. His research mainly focuses on the design and preparation of functional materials for energy storage and conversion.*

earth's crust and also environmentally benign. In addition, the semiconductor industry has a mature technology for large-scale production of Si. Because of these advantages, Si has been regarded as one of the most promising candidates for LIB anodes. Unfortunately, its large volume change (>300%) during cycling induces severe cracking of Si, electrical disconnection of the active materials from the current collector, as well as formation of an unstable solid electrolyte interphase (SEI) on the Si surface, consequently leading to fast capacity fade of the electrodes. Moreover, the slow lithium diffusion kinetics in Si (diffusion coefficient between $10^{-14}$ and $10^{-13}$ $cm^2$ $s^{-1}$) and the low intrinsic electric conductivity of Si (~$10^{-3}$ S $cm^{-1}$) affect significantly the rate capability and the full capacity utilization of Si electrodes.[18] These issues have to be addressed before the practical application of Si electrodes.

Recently, strategies, such as generation of nanostructures, surface modification, addition of electrolyte additives, development of novel polymer binders, and selection of appropriate current collectors, have been developed and proved to be efficient in improving the electrochemical performance of Si electrodes. Considerable efforts have been devoted to the generation of a variety of Si nanostructures, such as thin films, nanosheets, nanorods, nanotubes, and porous structures. Nanostructures have several advantages over bulk ones. (1) Nanostructures can relax the mechanical strain and effectively accommodate the volume variation during lithiation and delithation processes, maintaining high specific capacity with a significantly improved cycle life. (2) Nanostructures can provide much higher active surface area, permitting rapid interfacial $Li^+$ diffusion. (3) Nanostructures may shorten the diffusion distance for $Li^+$, ensuring reduced polarization and improved rate capability.[18,19] The incorporation of conductive species, such as carbonaceous materials, metals, and conductive polymers, has also been frequently employed to improve the electric conductivity, rate capability and cycling stability of Si electrode materials. In order to improve the performance of Si electrodes, electrolyte additives, binders, and current collectors involved in the electrode generation should be also considered. The addition of appropriate additives would control the formation of thin and stable SEI layers, reducing the consumption of extra electrolyte upon cycling and consequently leading to better cycling stability. Polymer binders are usually mixed with active materials and conductive additives to form slurries and help to form relatively homogeneous and stable coatings on current collectors. The selection of proper polymer binders would enhance the integrity of Si electrodes. In addition, current collectors with porous structures and rough surface are also essential to ensure good electric contact between active materials and current collectors.

In this review, we summarize the strategies developed recently for improving the electrochemical performance of these Si materials. The focus of this review is the recent progress in the controlled preparation of Si nanostructures with a variety of morphologies, including solid nanostructures, hollow nanostructures, and porous structures. Surface modification based on the incorporation of electronically conductive agents, such as carbonaceous materials, metals, and conductive polymers into Si nanostructures to improve the electrochemical performance are also discussed. Other factors that affect the performance of Si anodes, such as electrolyte additives, binders, and current collectors, are also presented. The opportunities and perspectives for future research on Si anodes in LIBs are outlined.

*Prof. Jie-Sheng Chen received his PhD degree from Jilin University in 1989 and worked as a postdoctoral fellow in the Royal Institution of Great Britain, the United Kingdom, from 1990 to 1994, and as a professor in the Department of Chemistry, Jilin University from 1994 to 2008, he has been a professor in the school of Chemistry and Chemical Engineering, Shanghai Jiao Tong University. His research interest is the synthesis of solid compounds and composite materials with new structures and functioins.*

## 2. Fabrication of Si nanostructures

Silicon nanostructures have many attractive properties, such as large specific surface area, high damage tolerance, fast electron transportation rate, and shortened $Li^+$ diffusion distance, demonstrating much improved electrochemical performance as anodes in LIBs. In this section, three types of Si nanostructures, including solid nanostructures, hollow nanostructures, and porous structures are discussed.

### 2.1 Solid Si nanostructures

#### Thin films

Thin films can significantly shorten $Li^+$ diffusion distance and effectively alleviate the pulverization caused by the volume expansion. In the last decade, great success has been made in the fabrication of Si thin film anodes with large specific capacity, good cycling stability, and high rate capability.[20-29] Generally, Si thin films are mainly fabricated by two traditional techniques, namely chemical vapour deposition (CVD) and physical vapour deposition (PVD). For example, amorphous Si (a-Si) thin film was prepared with CVD technique by using $Si_2H_6$ as source gas.[20] The maximum capacity of the film was more than 4000 mA h $g^{-1}$ at a constant current of 100 μA/$cm^2$. Moreover, cycling durability reached as high as 1500 cycles when the inserted charge amount was 430 mA h $g^{-1}$. Graetz *et al.*[22] fabricated a-Si thin films with thickness of approximately 100 nm by a PVD method. The films delivered a high initial discharge capacity of 3500 mA h $g^{-1}$ at a rate of 0.25 C and retained more than 1700 mA h $g^{-1}$ after 50 cycles, much better than crystalline Si nanoparticles.

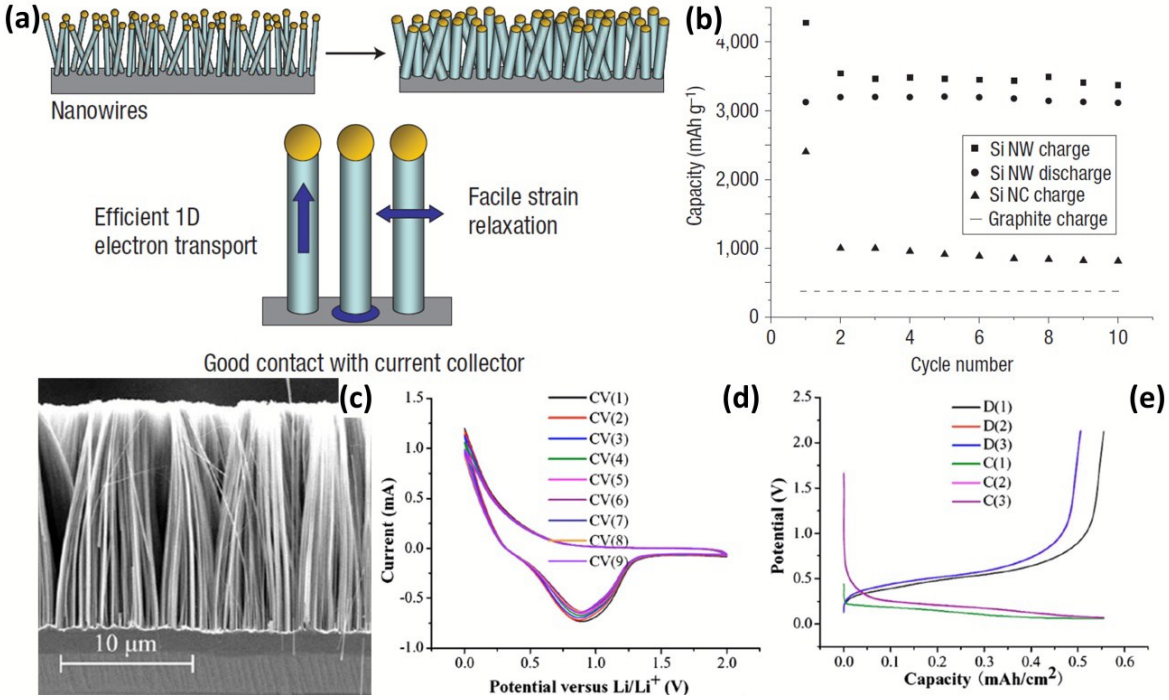


**Fig. 1** (a) Schematic of Si NWs grown directly on the current collector. (b) Capacity *versus* cycle number for the Si NWs at a rate of C/20. Reprinted with permission from ref. 30. Copyright 2008 Nature Publishing Group. (c) Typical cross-sectional SEM image of Si NWs arrays prepared by MCEE. (d) Typical cyclic voltammograms (CV) of the MCEE Si NWs. (e) Charge-discharge profiles of the MCEE Si NWs. Reprinted with permission from ref. 31. Copyright 2008 American Institute of Physics.

**Nanowires (NWs)**

NWs with high aspect ratio have many desired electrochemical features: (1) Small diameter of NWs is more resistant to cracking than bulk Si structures. (2) Direct one-dimensional electronic pathways in NWs allow for efficient charge transport. (3) The aggregation of NWs provides void space to accommodate the volume expansion during cycling. In 2008, Chan *et al*.[30] reported directly growth of Si NWs onto stainless steel current collectors by a vapour-liquid-solid (VLS) synthesis method (Fig. 1a). When these Si NWs used as anode materials, an exceptionally high initial lithiation capacity of 4277 mA h $g^{-1}$ was delivered at a rate of 0.05 C, and a constant capacity of over 3500 mA h $g^{-1}$ was retained up to 10 cycles (Fig. 1b). Recently, various Si NWs anodes with further enhanced electrochemical performance have been developed.[31-39] Fig. 1c shows the typical cross-section SEM image of Si NWs prepared by metal-catalyzed electroless etching (MCEE).[31] The MCEE Si NWs have good conductivity, ensuring efficient electron transport during charge/discharge processes. Furthermore, their rough surface allows for much better accommodation of huge volume change than the VLS Si NWs. The MCEE Si NWs exhibited a lithiation capacity of approximately 0.5 mA h $cm^{-2}$ and excellent cycling stability (Fig. 1d and e).

**Nanorods (NRs)**

The application of Si NRs in LIB anodes has been received extensive consideration.[40-45] For example, Si thin films were prepared on Cu foil substrates by CVD and modified by MCEE for the fabrication of Si NRs.[40,41] The Si NRs showed considerably better electrochemical performance than the pristine Si thin film. Moreover, Si NRs prepared by oblique-angle deposition (OAD) on Cu foils delivered a high initial reversible capacity of approximately 1500 mA h $g^{-1}$, and good capacity retention was achieved for 25 charge-discharge cycles.[42] The good electrochemical performance of these Si NRs is attributed to the nanostructure, which provides free vacancies to contain the volume variation and absorb the stress caused by the Li intercalation. However, special devices, harsh reaction conditions and multi-step procedures are usually involved in the above-mentioned synthetic methods for Si NRs. In 2007, Bao *et al*.[46] reported the fabrication of microporous Si by reducing microporous silica *via* a magnesiothermic reduction process. Using the same method, Si NRs composed of small nanocrystals were successfully prepared by reducing $SiO_2$ nanotubes.[43] In addition to the eco-friendly and facile synthetic route, these Si NRs displayed a significantly improved electrochemical performance compared to the bulk silicon and porous silicon networks. Discharged/charged at a current density of 0.2 A $g^{-1}$ for 170 cycles, a reversible capacity of approximately 1038 mA h $g^{-1}$ was still maintained.

**Nanosheets (NSs)**

NSs are also of great interest in LIB anodes due to its low dimensional features. First, the ultrathin Si NSs permit the fast kinetics of charge carrier and $Li^+$ diffusion. Second, the nanosheet structures may effectively buffer the strain generated during the lithiation/delithiation processes. Third, the large specific surface area allows effective contact

between the electrolyte and the electrode, contributing to the high specific capacities. For instance, Lu *et al.*[47] reported the preparation of ultrathin Si NSs by using graphene oxide (GO) as template. These Si NSs kept a discharge capacity of approximately 600 mA h $g^{-1}$ with a Coulombic efficiency of 96.2% after discharged/charged at a current density of 0.1 C for 100 cycles, demonstrating their good lithium storage properties. However, the fabrication of these Si NSs is quite complicated and the yield is very low. Recently, ultrathin Si NSs have been prepared by a scalable DC arc-discharge plasma method.[48] The thickness of Si NSs is less than 2.5 nm and the average size is about 20 nm. The NSs exhibited superior cycling stability and high rate capability.

## 2.2 Hollow Si nanostructures

### Nanotubes (NTs)

Si NTs are regarded as promising anode materials for LIBs. The axial tubes provide accessible channels for electrolyte transportation and additional space for the volume expansion during cycling. Furthermore, both inner and outer walls of NTs are exposed to the electrolyte, shortening lithium diffusion length. Park *et al.*[49] fabricated Si NTs by reductive decomposition of a Si precursor in an porous Al template. At a rate of 1 C, these NTs showed high reversible charge capacities of approximately 3200 mA h $g^{-1}$ with excellent capacity retention of 89% after 200 cycles. Yoo *et al.*[50] prepared Si NTs using electrospun polyacrylonitrile nanowires as templates. The electrochemical performance of the Si NTs was proved to be much better than those of commercial Si nanoparticles and Si NWs. At a current density of 0.4 mA $g^{-1}$, an initial discharge capacity of approximately 1900 mA h $g^{-1}$ was achieved and good capacity retention was also demonstrated. It is supposed that the pulverization issue can be addressed by introducing the above-mentioned nanotubular structures. However, the formation of the unstable SEI is still quite serious. Wu *et al.*[51] recently proposed novel double-walled Si-$SiO_x$ nanotubes (DWSi NTs) to prevent the formation of unstable SEI. Continuous Si NTs with an oxide coating layer on the outer surface were prepared by using an electrospun nanofiber templating method (schematically illustrated in Fig. 2a). The DWSi NTs showed much better electrochemical performance than Si NTs without oxide and Si NWs. In addition, high specific charge capacities (~2970 mA h $g^{-1}$ at C/5, 1000 mA h $g^{-1}$ at 12 C), long cycle life (6000 cycles with 88% capacity retention at 12 C), and high rate capability (up to 20 C) have been realized in the DWSi NTs. These highly desirable electrochemical parameters are attributed to the unique structure of these DWSi NTs. The outside $SiO_x$ coating layer is mechanically rigid and can prevent Si from expanding outward while still permitting $Li^+$ to pass through. Furthermore, the electrolyte does not wet inside the NTs due to the high aspect ratio of the continuous NTs. Thus, the outer surface of the NTs interfaced with the electrolyte is static, allowing for the generation of a stable SEI on the outer surface. The formation of stable SEI is confirmed by SEM image of NTs after 2000 cycles and impedance measurements for NTs after different numbers of cycles (Fig. 2b and c).

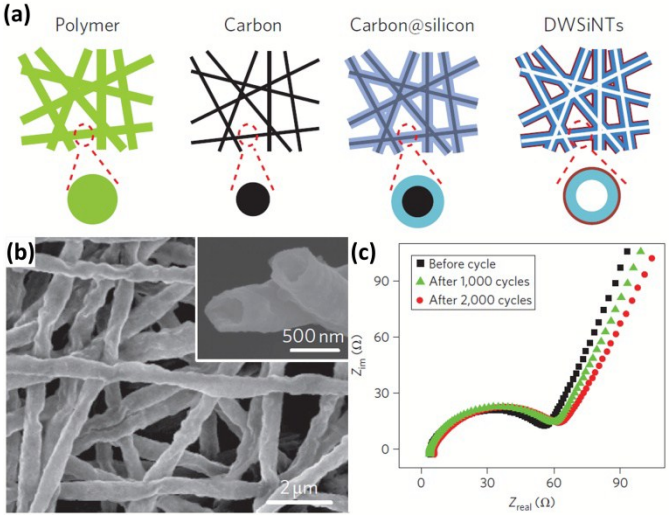


**Fig. 2** (a) Schematic of the preparation process for DWSi NTs. (b) SEM image of DWSi NTs after 2000 cycles, showing the NTs coated with a uniform thin SEI layer. (c) Impedance measurements for DWSi NTs after different numbers of cycles, indicating no significant growth of SEI during cycling. Reprinted with permission from ref. 51. Copyright 2012 Nature Publishing Group.

### Hollow spheres (HSs)

Si HSs have large inner void space, which can well accommodate the volume expansion and relieve the diffusion-induced stress during cycling. In addition, the thin shell of Si HSs can significantly shorten the diffusion distance for the $Li^+$ and electrolyte. Yao *et al.*[52] reported interconnected Si HSs prepared by CVD method by using $SiO_2$ spheres as hard templates (Fig. 3a). The Si HSs with an inner radius of approximately 175 nm and an outer radius of about 200 nm (Fig. 3b and c) show excellent electrochemical performance. An initial reversible capacity of as high as 2725 mA h $g^{-1}$ was achieved at a rate of 0.1 C and a discharge capacity of 1420 mA h $g^{-1}$ was obtained at 0.5 C for 700 cycles. Unfortunately, the whole CVD process which involves toxic $SiH_4$ and $SiO_2$ spheres is not feasible for mass production. Chen *et al.*[53] reported a scalable and simple method for the preparation of uniform Si HSs through magnesiothermic reduction of mesoporous silica HSs (Fig. 3d). The Si HSs have an average diameter and shell thickness of approximately 120 and 20 nm, respectively (Fig. 3e and f). The Si HSs displayed improved electrochemical performance compared to commercial Si nanoparticles.

## 2.3 Porous Si structures

The introduction of a porous structure to the Si anode has been proven to be a highly efficient strategy to improve the electrochemical performance of Si materials.[54-68] The pores of these Si materials can effectively buffer the large volume expansion upon lithiation, contributing to better cycling performance. In addition, the porous structure can facilitate the transport of $Li^+$ and electrolyte, benefiting to the rate performance. Roughly, there are two types of methods in the

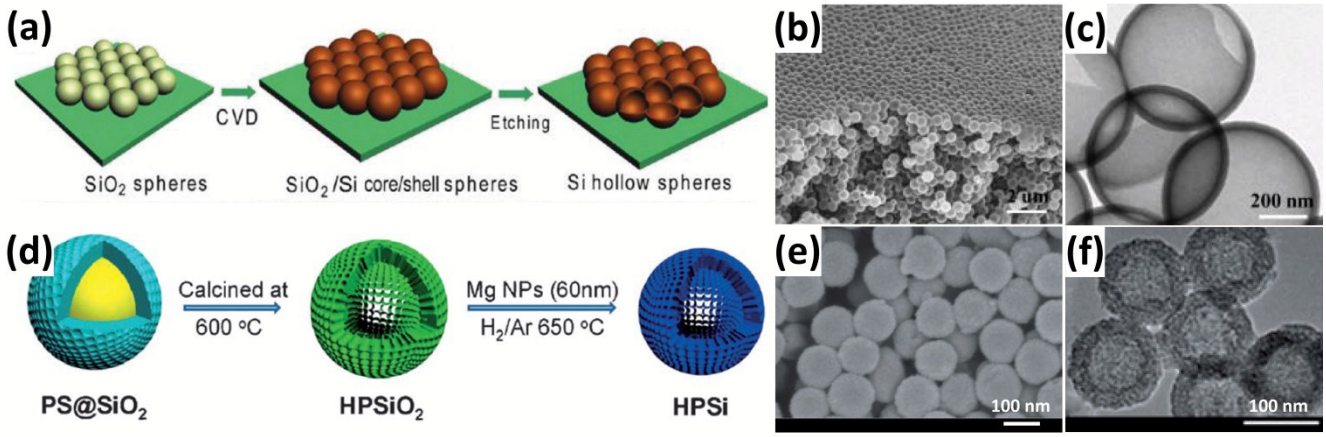


**Fig. 3** (a) Schematic illustration of the preparation of Si HSs. (b, c) SEM and TEM images of Si HSs prepared by a CVD method. Reprinted with permission from ref. 52. Copyright 2011 American Chemical Society. (d) Schematic diagram of the procedure to prepare Si HSs. (e, f) SEM and TEM images of Si HSs prepared by a magnesiothermic reduction method. Reprinted with permission from ref. 53. Copyright 2012 WILEY-VCH Verlag GmbH & Co. KGaA, Weinheim.

fabrication of porous Si materials, non-template approach and template-assisted approach.[69]

**Non-template approach**

Electroless etching *via* a galvanic displacement between Si and metal particles is an effective way to produce porous Si. For example, Ge *et al*.[54] fabricated porous Si nanoparticles by a two-step approach combining boron doping and Ag-assisted chemical etching (Fig. 4a). The porosity of these porous Si nanoparticles can be controlled by adjusting the ratio of Si and boric acid during the doping procedure (Fig. 4b-d). Bang *et al*.[55] reported the preparation of porous Si by a similar etching method (Fig. 4e). The Si has a three-dimensional (3D) porous structure with pore size of hundreds nanometres, and an average particle size of approximately 7 μm (Fig. 4f-h). Ge *et al*.[56] prepared porous Si particles from bulk metallurgical Si by a two-step approach combining ball milling and Fe-assisted chemical etching (Fig. 4i). The pores with a size of around 3 nm are uniformly distributed over the surface of bulk Si (Fig. 4j and k). The electrochemical performance of the porous Si is much superior over the non-porous bulk Si substrate.

**Template-assisted approach**

Monodispersed $SiO_2$ nanospheres with tunable particle size

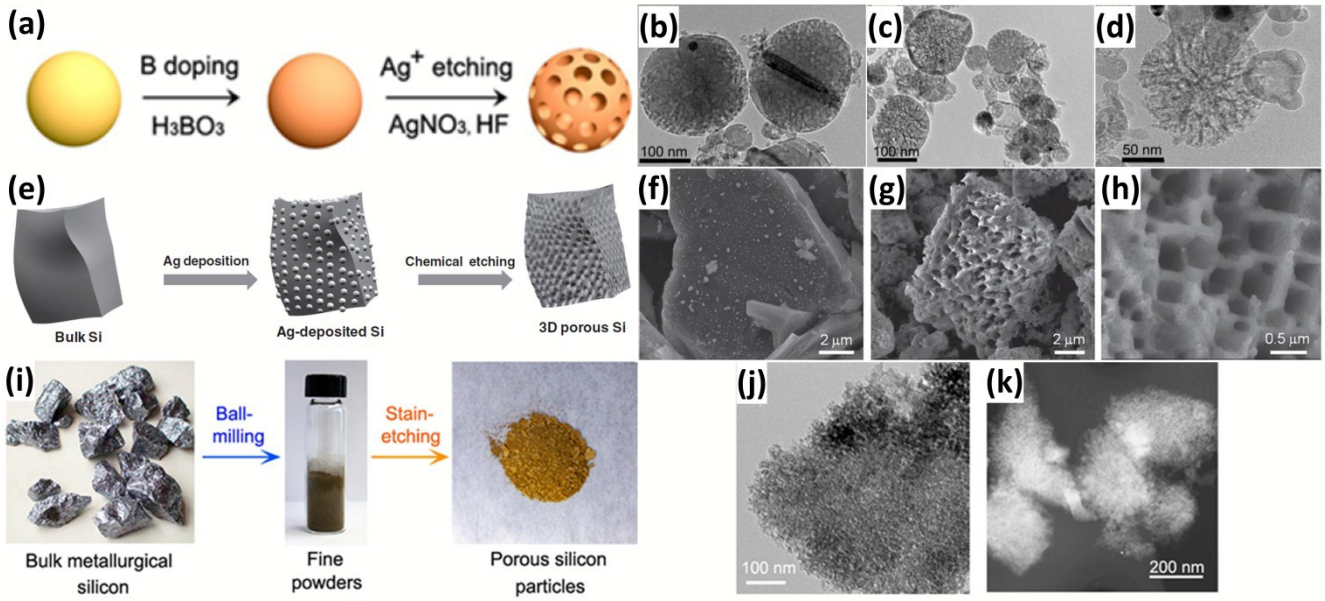


**Fig. 4** (a) Schematic illustration of the preparation of porous Si nanoparticles. TEM images of porous Si nanoparticles prepared with initial $H_3BO_3$: Si mass ratios of 2:5 (b), 4:5 (c), and 8:5 (d), respectively. Reprinted with permission from ref. 54. Copyright 2013 Springer. (e) Schematic diagram of the procedure to prepare porous bulk Si. (f) SEM image of Ag-deposited Si. (g, h) SEM images of chemically etched Si. Reprinted with permission from ref. 55. Copyright 2012 WILEY-VCH Verlag GmbH & Co. KGaA, Weinheim. (i) Synthetic route of porous Si from metallurgical Si by a two-step approach combining ball milling and Fe-assisted chemical etching. (j) TEM image of porous Si particles. (K) STEM image of porous particles. Reprinted with permission from ref. 56. Copyright 2013 American Chemical Society.

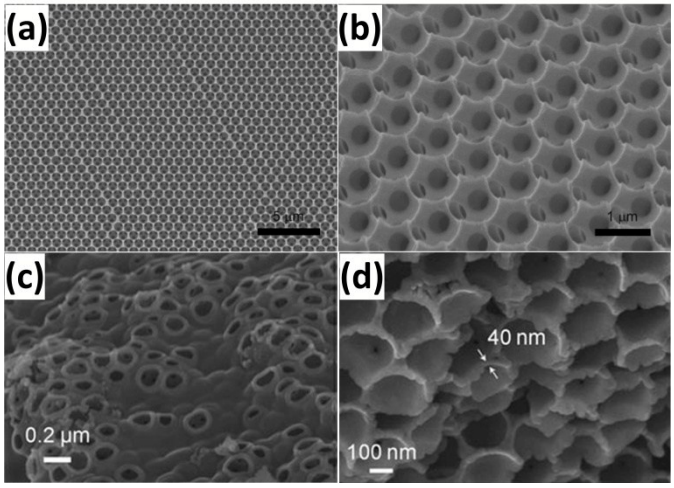


**Fig. 5** (a, b) SEM images of porous Si templated from 890 nm pre-sintered $SiO_2$ spheres. Reprinted with permission from ref. 57. Copyright 2009 WILEY-VCH Verlag GmbH & Co. KGaA, Weinheim. (c, d) SEM images of 3D porous Si prepared by reduction of $SiCl_4$ with a $SiO_2$ template. Reprinted with permission from ref. 58. Copyright 2008 WILEY-VCH Verlag GmbH & Co. KGaA, Weinheim.

are widely used as sacrificial hard templates to form porous Si structures. For example, Esmanski *et al*.[57] reported a porous Si prepared by CVD with $SiO_2$ hard templates. Typically, monodispersed $SiO_2$ spheres with a diameter of 890 nm were first prepared by a modified Stöber method, and then deposited onto a substrate *via* an evaporation-induced self-assembly method. Hydrogenated amorphous Si was then deposited in the interstices of $SiO_2$ spheres by dynamic cold-wall low-pressure CVD by using $Si_2H_6$ as a Si source. The porous Si was finally obtained by dissolving $SiO_2$ in HF solution (Fig. 5a and b). In another example, $SiO_2$ sphere template was mixed with Si gel formed by reducing $SiCl_4$ with sodium naphthalide and annealed at elevated temperature. A porous Si material was obtained after HF treatment (Fig. 5c and d).[58] This Si material with a 3D interconnected porous structure had good capacity retention of 90% up to 100 cycles at a rate of 1 C.

In addition to sacrificial template method, self-templating is also an efficient approach to generate porous Si structures. Mesoporous $SiO_2$ materials can serve as both templates and silicon sources. Many porous Si materials have been generated through the magnesiothermic reduction of mesoporous $SiO_2$. Typically, $SiO_2$ powder is mixed with magnesium powder and then heated in a tube furnace. When the temperature reaches 650 °C, molten magnesium would be imbibed into the pores and reacted with $SiO_2$ to form MgO-Si nanocomposite. Porous Si materials are acquired by the removal of MgO and residual $SiO_2$ by acid. For instance, Yu *et al*.[59] reported the preparation of porous Si *via* reduction of mesoporous $SiO_2$ with a pore diameter of approximately 10 nm. The obtained Si particles have a coherent macroscopic porous network with pores of about 200 nm diameter and wall thickness ranging from 150 to 250 nm (Fig. 6a and b). Since then, highly ordered mesoporous $SiO_2$ materials, such as SBA-15[60] and KIT-6[61], were also used as precursors to prepare porous Si by this magnesiothermic reduction method. The porous Si particles with the original morphology of mesoporous $SiO_2$ have porous structures

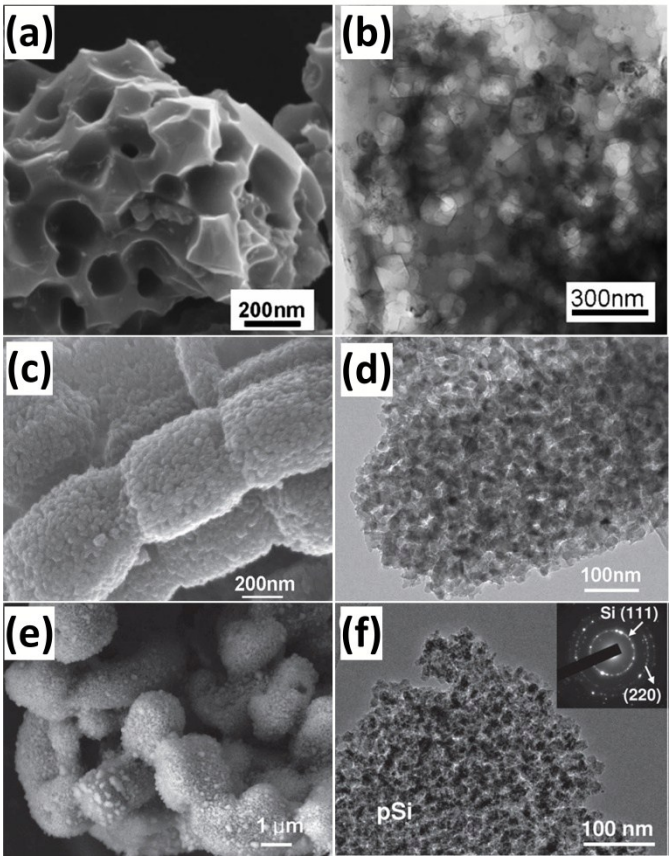


**Fig. 6** (a, b) SEM and TEM images of porous Si templated from mesoporous $SiO_2$ powder. Reprinted with permission from ref. 59. Copyright 2010 WILEY-VCH Verlag GmbH & Co. KGaA, Weinheim. (c, d) SEM and TEM images of porous Si templated from SBA-15. Reprinted with permission from ref. 60. Copyright 2011 WILEY-VCH Verlag GmbH & Co. KGaA, Weinheim. (e, f) SEM and TEM images of porous Si templated from KIT-6. Reprinted with permission from ref. 61. Copyright 2011 Royal Society of Chemistry.

composed of homogeneously distributed primary Si crystallites with the size of 20-30 nm (Fig.6c-f). Moreover, the high specific surface areas of these porous Si particles are favourable for the fast electrode kinetic. More recently, natural reservoirs with high contents of $SiO_2$ and large numbers of pores, such as rice husk[62-64] and diatomite,[65,66] have also been used as raw materials for the preparation of porous Si. As revealed by the charge/discharge test, the porous Si showed much better electrochemical performance than commercial Si nanoparticles due to the presence of the porous structures. Table 1 summarizes the most recent electrochemical data on Si nanostructures for LIB anodes reported in the literature.

## 3. Formation of Si composites

Introducing hollow and porous structures have been proved to be efficient in addressing the issues of Si electrodes, such as volume expansion upon lithiation, diffusion distance of lithium ions, and diffusion-induced stress. However, due to the high porosity and specific surface area, these structures usually have very low tap densities and consequently result in low

**Table 1** Synthetic strategies and electrochemical properties of Si nanostructure anode materials in LIBs

| Sample | Methods | Initial reversible capacity (mA h $g^{-1}$) | Initial Coulombic efficiency (%) | Capacity (mA h $g^{-1}$) | References |
|---|---|---|---|---|---|
| Si thin films | Electrodepositing | 2550 at 0.36 A $g^{-1}$ | 53 | 2800 after 80 cycles | 23 |
| Si thin films | PECVD | 2875 at 1 C | 50 | 2100 after 100 cycles | 25 |
| Si thin films | Magnetron sputtering | 3134 at 0.025 C | 87 | 1317 at 0.5 C after 500 cycles | 27 |
| Si NWs | VLS-CVD | 3124 at 0.05 C | 73 | 3250 after 10 cycles | 30 |
| Si NWs | HF-CVD | 3720 at 0.1 C | 65 | 2670 at 1.3 C after 50 cycles | 34 |
| Si NWs | CVD | 1640 at 0.2 C | 79 | 1300 after 100 cycles | 35 |
| Si NWs | VLS-CVD | 2836 at 0.1 C | 93.7 | 2600 after 20 cycles | 38 |
| Si NWs | PECVD | 3500 at 0.05 C | 96 | 2930 at 0.5 C after 50 cycles | 39 |
| Si NRs | ECR-CVD/MCEE | 2911 at 0.25 mA $cm^{-2}$ | 95 | 2445 after 25 cycles | 40 |
| Si NRs | ECR-MOCVD/MCEE | 2990 at 0.15 C | 92 | 1420 after 100 cycles | 41 |
| Si NRs | Magnesiothermic reduction | 1586 at 0.2 A $g^{-1}$ | 48.3 | 1038 after 170 cycles | 43 |
| Si NRs | RF-PECVD/DRIE | 2348 at 1.2 C | 60 | 1244 after 25 cycles | 45 |
| Si NSs | Magnesiothermic reduction | — | — | 600 at 0.1 C after 100 cycles | 47 |
| Si NSs | DC arc-discharge plasma | 1242 at 0.1 A $g^{-1}$ | 49 | 442 after 40 cycles | 48 |
| Si NTs | Electrospinning/CVD | 650 at 12 C | 76 | 570 after 6000 cycles | 51 |
| Si HSs | CVD | 2725 at 0.1 C | 77 | 1420 at 0.5 C after 700 cycles | 52 |
| Si HSs | Magnesiothermic reduction | — | — | 1750 at 0.5 A $g^{-1}$ after 50 cycles | 53 |
| Porous Si | MCEE of Si powders | 1780 at 0.1 C | 69.3 | 125 after 30 cycles | 55 |
| Porous Si | MCEE of bulk metallurgical Si | — | — | > 1400 at 0.2 C after 160 cycles | 56 |
| Porous Si | CVD with $SiO_2$ hard templates | 2698 at 0.1 C | 87.2 | 2000 after 145 cycles | 57 |
| Porous Si | Magnesiothermic reduction of mesporous $SiO_2$ | 2416 at 0.1 A $g^{-1}$ | 73.7 | 1600 after 100 cycles | 59 |
| Porous Si | Magnesiohermic reduction of rice husk | 2790 at 84 mA $g^{-1}$ | 70 | 1500 at 2.1 A $g^{-1}$ after 300 cycles | 63 |
| Porous Si | Magnesiothermic reduction of diatomite | 1826 at 50 mA $g^{-1}$ | 68.5 | 240 after 30 cycles | 65 |

volumetric energy density. Given this fact, Si NPs with high tap densities are regarded as practically applicable anode materials for LIBs. In addition, Si NPs are commercially available and compatible with the current slurry coating manufacturing process for LIB electrodes. However, unlike other Si nanostructures described in Section 2, Si NPs are prone to pulverization during cycling, leading to rapid capacity loss. Thus, Si NPs cannot be directly used for a LIB electrode. To address these issues, many conductive agents, such as carbonaceous materials, metals, and polymers, have been incorporated into Si NPs.

### 3.1 Incorporation of carbonaceous materials

#### Carbon coatings

The formation of carbon coatings has been widely exploited and considered as an efficient method to enhance the electrochemical performance of Si NPs. The carbon coating improves the electric conductivity and restricts the volume change of Si upon cycling. In addition, such coating also allows for the formation of a stable SEI upon cycling and prevents the deterioration of the electrode performance. Various methods, such as CVD by using toluene or propylene gas[70-72] and pyrolysis of carbonaceous precursors,[73-90] have been employed to fabricate carbon coatings on the surface of Si NPs. Magasinski *et al.*[70] prepared Si NPs/carbon composite granules through hierarchical bottom-up assembly. As illustrated in Fig. 7a, carbon-black nanoparticles were branched into short chains by high-temperature pre-annealing. Si NPs were then deposited onto the annealed carbon-black by a CVD method employing $SiH_4$ as a Si source. The multibranched nanocomposite was finally self-assembled into large porous spherical granules during the following carbon deposition. The produced spheres have particle sizes ranging from 15 to 30 µm (Fig. 7b and c) and pore sizes of 30-100 nm in diameter (Fig. 7d and e). The incorporation of carbon and the presence of porous structure endow the Si NPs/carbon composite granules with high electrochemical performance. A high reversible capacity of 1950 mA h $g^{-1}$ is achieved at C/20 and a capacity close to 82% of this maximum is maintained at 1 C over 100 cycles (Fig. 7f). Recently, yolk-shell structures have been widely investigated for further improving the performance of Si NPs/carbon composites. Liu *et al.*[73] reported the preparation of a pomegranate-like Si NPs/C composite by a polymer-pyrolysis method. As illustrated in Fig. 7g, commercial Si NPs coated with a $SiO_2$ layer were mixed with emulsifier to form water-in-oil emulsions. A resorcinol-formaldehyde (RF) resin layer was generated on the surface of assembled Si@$SiO_2$ nanoparticle clusters, and then converted into a carbon coating by a carbonization process. After the removal of $SiO_2$ with HF solution, pomegranate-like Si NPs/C composite with plenty of void space between the Si NPs and carbon coating was generated (Fig. 7h-j). Due to the carbon coating and yolk-shell structure, the composite showed much better electrochemical performance than raw Si and Si cluster@C (Fig. 7k). A reversible capacity of 2350 mA h $g^{-1}$ was achieved at a

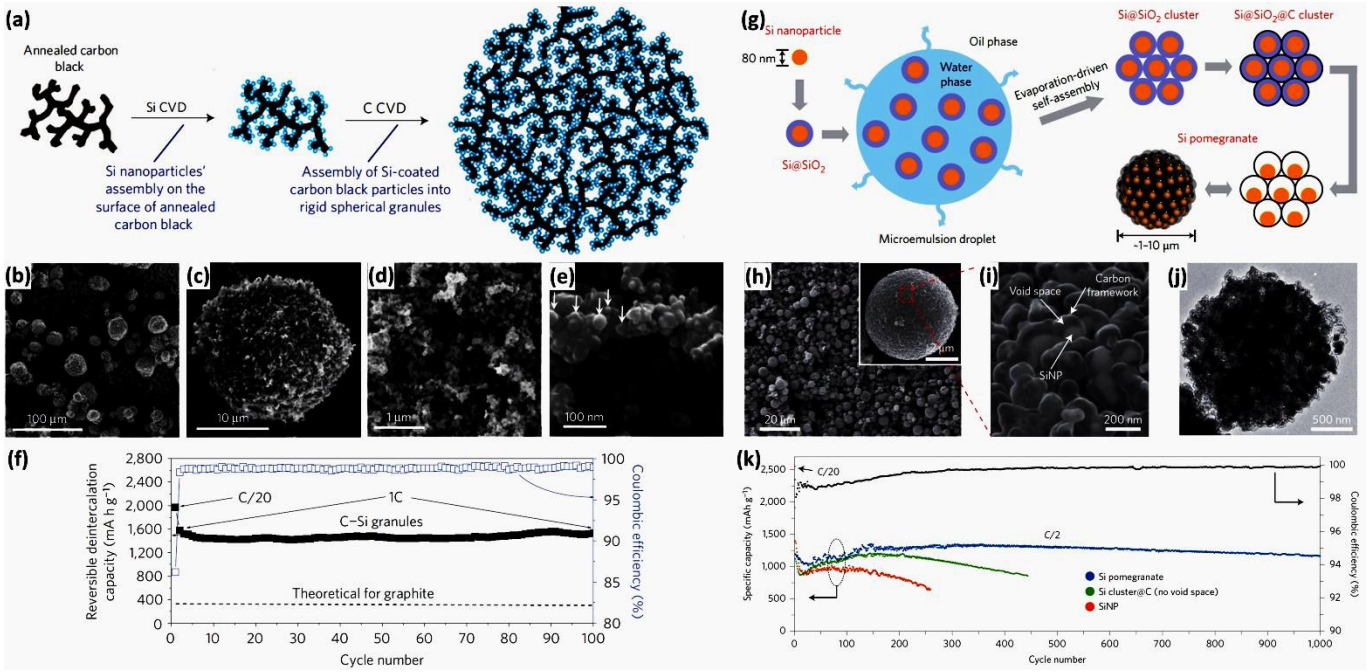


**Fig. 7** (a) Schematic of Si NPs/carbon composite granules formation *via* hierarchical bottom-up assembly. (b-e) SEM images of the Si NPs/carbon composite granules recorded at different magnifications. (f) Coulombic efficiency and reversible Li deintercalation capacity of the Si NPs/carbon composite granules *versus* cycle number. Reprinted with permission from ref. 70. Copyright 2010 Nature Publishing Group. (g) Schematic of the fabrication process for silicon pomegranates. (h, i) SEM images of the Si pomegranates recorded at different magnifications. (j) TEM image of one Si pomegranate particle. (k) Cycling performance of Si pomegranates, Si cluster@C, and Si NPs under the same conditions. Coulombic efficiency is plotted for the Si pomegranates only. Reprinted with permission from ref. 73. Copyright 2014 Nature Publishing Group.

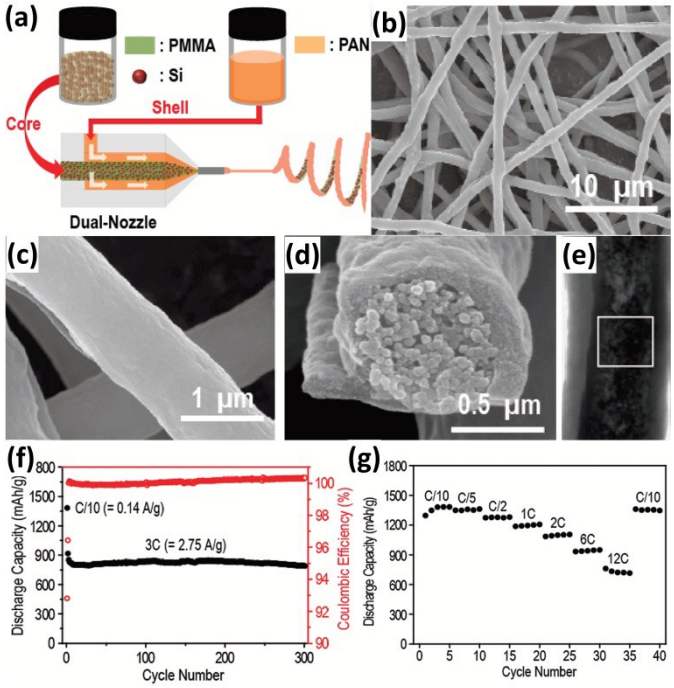


**Fig. 8** (a) Schematic illustration of the electrospinning process. SEM images of Si NPs/CNFs composite at (b) low and (c) high magnifications. (d) A cross-sectional SEM view of a single Si NPs/CNF. (e) A TEM image of a single Si NPs/CNF. (f) Cycling performance of the Si NPs/CNFs composite measured at 3C rate (2.748 A/g). (g) Rate capability test for Si NPs/CNFs composite. Reprinted with permission from ref. 91. Copyright 2011 American Chemical Society.

rate of C/20. From the second to 1000th cycle at a rate of C/2, the capacity retention was more than 97%. Su *et al.*[89] also fabricated yolk-shell Si@void@C nanocomposites *via* a facile RF coating and subsequent LiOH etching. The nanocomposites showed much better electrochemical behaviors than raw Si and Si@C.

### Carbon nanofibers

Encapsulating into carbon nanofibers (CNFs) has also been regarded as an efficient approach to improve the electrochemical performance of Si NPs.[91-101] Electrospinning is the most common way to prepare Si NPs/CNFs composites. Hwang *et al.*[91] developed an electrospinning process to produce a Si NPs/CNFs composite using a dual nozzle (Fig. 8a). Si NPs and poly (methyl methacrylate) in N, N-dimethylformamide (DMF) and acetone were injected into the core channel of the nozzle. Polyacrylonitrile (PAN) dissolved in DMF was injected into the shell channel of the nozzle. After carbonization following the electrospinning process, Si NPs/CNFs composite with diameter of about 1 μm was generated (Fig. 8b and c). The Si NPs were completely wrapped by carbon shell, forming a core-shell structure (Fig. 8d and e). The carbon shell not only alleviates the large volume expansion of Si NPs but also promotes the electronic transportation of the electrode through the formation of a conductive network. In addition, the carbon shell can reduce the surface contact of NPs with the electrolyte and prevent the pulverization of Si NPs during cycling. The Si NPs/CNFs composite exhibited excellent cycling and rate performance. Cycled at a rate of 3 C, only 1% of the initial capacity was lost after 300 cycles (Fig. 8f). Increasing the rate from C/10 to 12 C, 52.2% of the original capacity was still maintained (Fig. 8g).

### Carbon nanotubes

Carbon nanotubes (CNTs) with properties of high electric conductivity, large accessible surface area, good mechanical properties, and chemical stability are a promising electrode material. The incorporation of CNTs can improve the electric conductivity of electrode and prevent the aggregation of Si

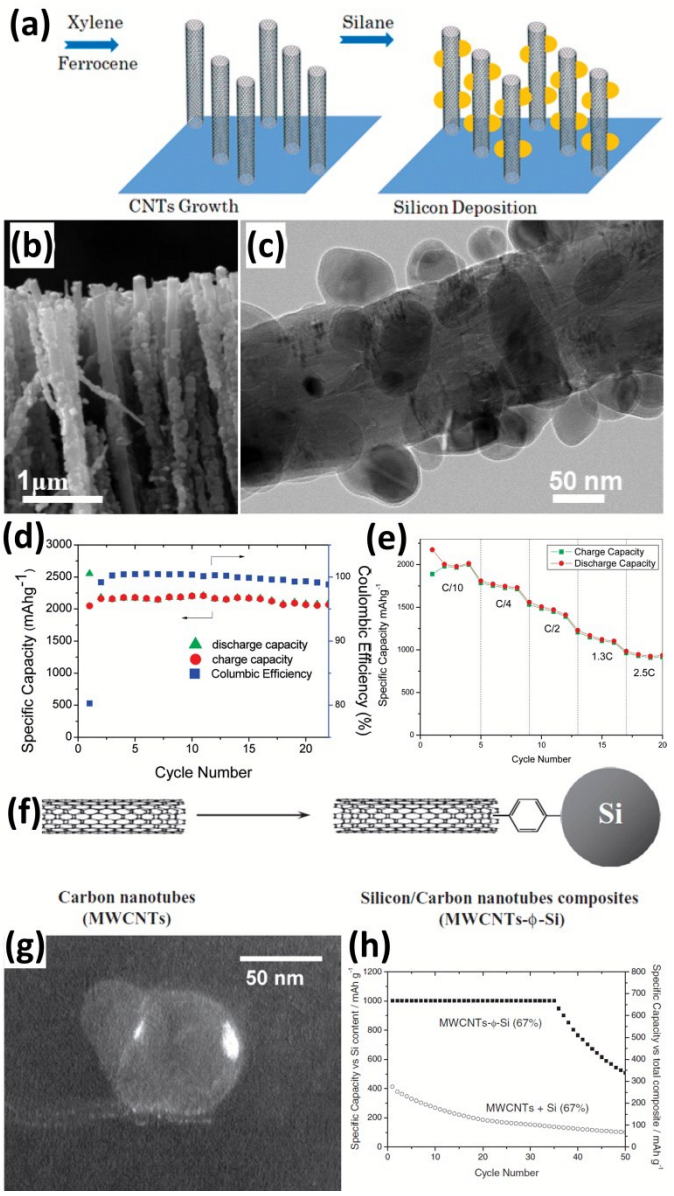


**Fig. 9** (a) Schematic diagram showing the preparation of Si NPs/CNTs composite. (b) SEM image of the Si NPs/CNTs composite. (c) TEM image of a single Si NPs/CNT. (d) Cycling performance of the Si NPs/CNTs composite at a current density of 100 mA $g^{-1}$. (e) Rate capability of the Si NPs/CNTs composite. Reprinted with permission from ref. 102. Copyright 2010 American Chemical Society. (f) Preparation of Si NPs/CNTs composite *via* a phenyl bridge. (g) Dark-field image of Si NPs showing that the particles are not only attached to the edge of CNTs but also by the walls. (h) Cycling performance of the Si NPs/CNTs composite at a current density of 0.5 A $g^{-1}$. Reprinted with permission from ref. 103. Copyright 2011 WILEY-VCH Verlag GmbH & Co. KGaA, Weinheim.

during cycling, leading to improved performance for the Si NPs/CNTs composites.[102-113] For example, Wang *et al*.[102] prepared a Si NPs/CNTs composite by a simple two-step CVD. As illustrated in Fig. 9a, the CNTs with an average diameter of 40-50 nm were first grown on quartz slides in a liquid injection based CVD reactor with xylene as the carbon source and ferrocene as the catalyst. Si NPs were then deposited onto CNTs by using $SiH_4$ as a Si source (Fig. 9b and c). The Si NPs/CNTs composite maintained a capacity of over 2000 mA h $g^{-1}$ at a current density of 100 mA $g^{-1}$ after 25 cycles (Fig. 9d). Increasing the current rate to 2.5 C, a capacity of approximately 1000 mA h $g^{-1}$ was achieved, demonstrating high rate capability (Fig. 9e). Si NPs/CNTs composite can also be prepared by mixing of pretreated Si NPs and aminophenyl-grafted CNTs in acetonitrile and the subsequent addition of tert-butylnitrite, forming closely binding of Si NPs and CNTs (Fig. 9f and g).[103] After grafting with CNTs, a capacity of 1000 mA h $g^{-1}$ was achieved for these Si NPs at a current density of 0.5 A $g^{-1}$ after 35 cycles (Fig. 9h).

**Graphene nanosheets**

Graphene (G) itself shows a low reversible capacity as an insertion host of LIBs. If used as a conducting and buffering matrix, G can greatly improve the electrochemical performance of Si NPs.[114-134] G can reduce surface contact of NPs with the electrolyte and improve the electric conductivity of electrode. Furthermore, the void space between the Si NPs and G can accommodate the volume variation during cycling, maintaining the integrity of the electrode. Researchers have developed several approaches to fabricate Si NPs/G composites for LIBs. For instance, Chabot *et al*.[114] reported the preparation of Si NPs/G composite by simply combining freeze-drying and thermal reduction processes (Fig. 10a). Si NPs were mixed with GO aqueous dispersion and sonicated for five hours. After lyophilized and subsequently treated in a tube furnace at 700 °C for 3 h under an Ar atmosphere containing 10 vol% $H_2$, Si NPs/G composite was obtained. SEM image shows that well-distributed Si NPs are wrapped by G (Fig. 10b). The composite achieved an initial discharge capacity of 2312 mA h $g^{-1}$ with 78.7% capacity retention after 100 cycles. Si NPs/G composite has also been fabricated through an *in-situ* pyrolysis and metal-catalyzed graphitization reaction (Fig. 10c).[115] Si NPs were first coated by an Ag sacrificial layer *via* a modified silver mirror reaction. The uniformly mixed Si@Ag composite, glucose and $FeSO_4$ were transferred into a tube furnace and heated up to 750 °C for 6 h under an $Ar/H_2$

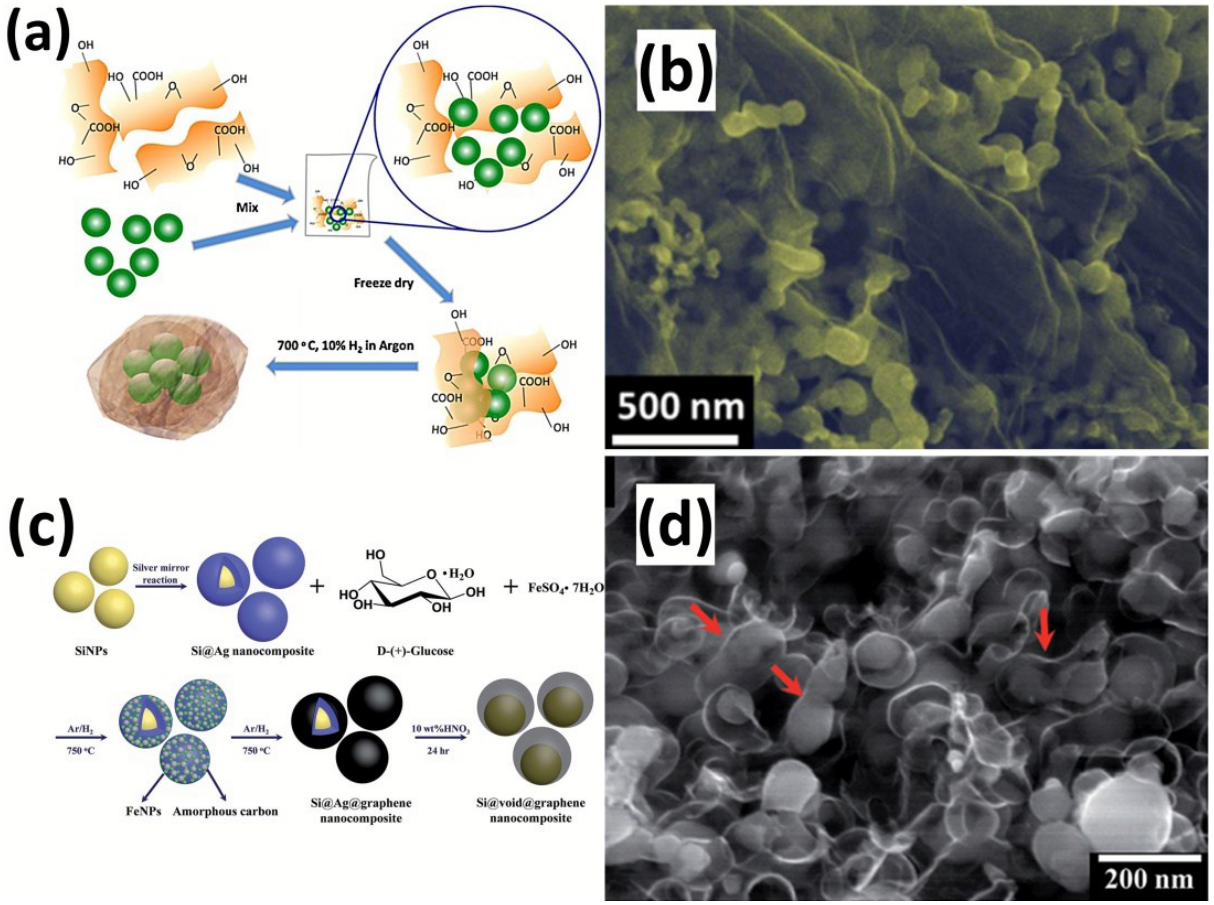


**Fig. 10** (a) Schematic view for preparation of the Si NPs/G composite. (b) SEM image of the Si NPs/G composite. Reprinted with permission from ref. 114. Copyright 2014 Elsevier. (c) Schematic diagram of the synthesis process of the Si NPs/G composite. (d) SEM image of the Si NPs/G composite. Reprinted with permission from ref. 115. Copyright 2015 Royal Society of Chemistry.

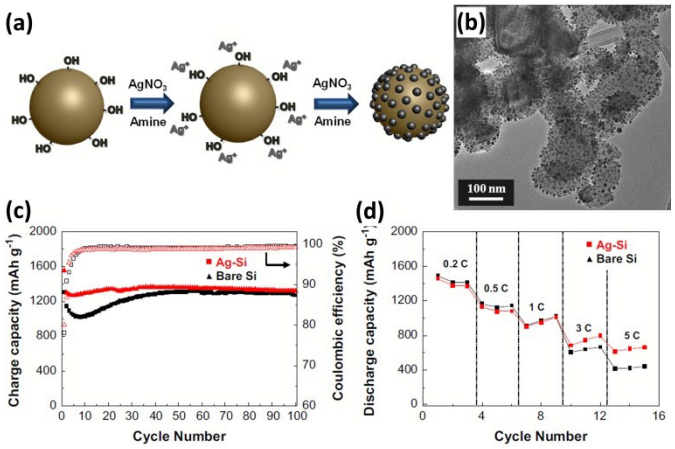


**Fig. 11** (a) Schematic illustration showing the preparation of Si NPs/Ag composite. ( b) TEM image of the Si NP s/Ag composite. (c) Cycling performance and (d) rate capability (0.2-10 C rates) of bare Si and Si NPs/Ag composite. Reprinted with permission from ref. 135. Copyright 2014 Elsevier.

atmosphere. After etching away the Ag layer in acid, Si NPs/G composite was obtained. Voids ranging from 35 to 43 nm between the Si NP core and G shell are clearly observed (Fig. 10d). A high capacity of 1410 mA h $g^{-1}$ was retained even after 600 cycles, indicating high cycling stability of this composite.

### 3.2 Incorporation of metal nanoparticles

Surface modification by metal nanoparticles such as Cu and Ag has been frequently adopted to improve the electrochemical performance, particularly Coulombic efficiency and rate capability of Si NPs.[135-138] The metal nanoparticle coating layers can enhance the surface electrical conductivity of Si, offering electron percolation paths from the current collector to the whole surface area of each individual Si nanoparticle. These coating layers can also prevent the aggregation of Si NPs and reduce surface contact of NPs with the electrolyte, forming a stable SEI layer. Employing butylamine as a reducing agent and $AgNO_3$ as an Ag precursor, Ag nanoparticles with an average diameter of 13 nm are uniformly anchored on a surface of Si NPs (Fig. 11a and b).[135] Due to the modification of Ag nanoparticles, the electrochemical properties of the Si NPs/Ag composite are much superior over that of the Si NPs alone. The initial Coulombic efficiency increased from 76.9% to 80%. A charge capacity of 1320 mA g $h^{-1}$ was still maintained at a rate of 0.2 C for 100 cycles, corresponding to nearly 100% capacity retention against at the second cycle (Fig. 11c). The composite also showed high rate capability. At a high rate of 5C, the capacity retention of 46.4% could be achieved (Fig. 11d).

### 3.3 Conductive polymers

Conductive polymers have many attractive features, including good electrical conductivity, high structural flexibility and superior chemical stability. Conductive polymers, such as polypyrrole (PPy) and polyaniline (PANi) have been widely employed to improve the electrochemical performance of Si

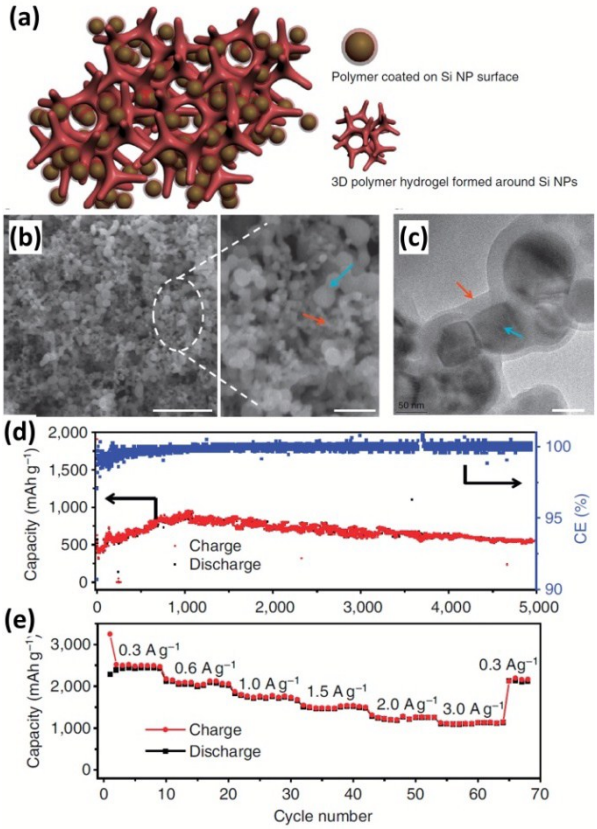


**Fig. 12** (a) Schematic illustration of 3D porous Si NP/PANi hydrogel composite. (b) SEM image of the Si NPs/PANi composite at low (left) and high (right) magnification. Scale bar, 1 μm (left) and 200 nm (right). (c) TEM image of the Si NPs/PANi composite. Scale bar, 50 nm. (d) Cycling performance of the Si NPs/PANi composite at a current density of 6.0 A $g^{-1}$ for 5000 cycles. (e) Rate capability of the Si NPs/PANi composite. Reprinted with permission from ref. 140. Copyright 2013 Nature Publishing Group.

NPs.[139-147] In 2005, PPy was incorporated into Si NPs *via* a high-energy mechanical milling process by Guo *et al*.[139] The obtained Si NPs/PPy composite showed enhanced electrochemical performance. However, it is hard to form uniform PPy coating on the surface of Si NPs by simple mechanical milling, impacting on the formation of continuous electronic transport pathway. Recently, Wu *et al*.[140] reported the incorporation of PANi hydrogel into Si NPs by an *in-situ* chemical polymerization technique. The Si NPs encapsulated by a conformal PANi layer are well distributed inside the highly porous PANi matrix (Fig. 12a-c). Moreover, the obtained Si NPs/PANi gel could be directly bladed onto a current collector without using any binder and conducting particles. A capacity of approximately 550 mA h $g^{-1}$ was achieved at a current density of as high as 6.0 A $g^{-1}$ for 5000 cycles, corresponding to 91% capacity retention (Fig. 12d). In addition, the capacity varied from 2500 to 1100 mA $h^{-1}$ at charge/discharge rate from 0.3 to 3.0 A $g^{-1}$, demonstrating excellent rate capability (Fig. 12e). The exceptional electrochemical performance of the Si NPs/PANi composite is attributed to its unique structure. First, the porous hydrogel matrix has empty space to allow for the huge volume expansion of the Si NPs during cycling. Second, the incorporation of PANi prevents the aggregation of Si NPs and reduces the surface contact of Si NPs with the electrolyte,

**Table 2** Synthetic strategies and electrochemical characteristics of Si NPs-based composites in LIBs

| Sample | Methods | Si content (wt%) | Initial reversible capacity (mA h $g^{-1}$) | Initial Coulombic efficiency (%) | Capacity (mA h $g^{-1}$) | References |
|---|---|---|---|---|---|---|
| Si NPs/C | CVD | 70.4 | 1850 at 0.1 A $g^{-1}$ | 80.1 | 1600 at 0.3 A $g^{-1}$ after 70 cycles | 71 |
| Si NPs/C | CVD | 37 | 783 at 0.1 A $g^{-1}$ | 57.1 | 767 after 100 cycles | 72 |
| Si NPs/C | Pyrolysis | 77 | 2350 at C/20 | 75 | 1160 at 0.5 C after 1000 cycles | 73 |
| Si NPs/C | Pyrolysis | 42 | 902 at 0.1 A $g^{-1}$ | 57 | 678 at 0.1 A $g^{-1}$ after 50 cycles | 74 |
| Si NPs/C | Pyrolysis | 58.9 | 759 at 0.1 A $g^{-1}$ | 41 | 1000 after 100 cycles | 78 |
| Si NPs/C | Pyrolysis | 71 | 2833 at 0.1 C | 60 | 1110 at 1 C after 1000 cycles | 88 |
| Si NPs/CNFs | Electrospinning | 50 | 1305 at 0.1 C | 87.5 | 750 at 3 C after 300 cycles | 91 |
| Si NPs/CNFs | Electrospinning | 50.2 | 1598 at 0.5 A $g^{-1}$ | 60.5 | 1104 after 100 cycles | 92 |
| Si NPs/CNFs | Electrospinning | 26.3 | 962 at 0.05 A $g^{-1}$ | 77.1 | 647 after 50 cycles | 100 |
| Si NPs/CNFs | Electrospinning | — | 886 at 0.05 A $g^{-1}$ | 76.3 | 452 after 50 cycles | 101 |
| Si NPs/CNFs | CVD | 32 | 1448 at 0.1 A $g^{-1}$ | 71 | 1042 after 20 cycles | 96 |
| Si NPs/CNTs | CVD | — | 2049 at 0.1 A $g^{-1}$ | 80.3 | 2000 after 25 cycles | 102 |
| Si NPs/CNTs | CVD | 59.6 | 860 at 0.05 C | 63 | 602 after 140 cycles | 113 |
| Si NPs/CNTs | Ball milling | 50 | 1601 at 0.2 A $g^{-1}$ | 66 | 757 after 30 cycles | 110 |
| Si NPs/G | Metal-catalyzed graphitization | 89.5 | 2411 at 0.05 C | 65 | 1410 at 0.5 C after 600 cycles | 115 |
| Si NPs/G | Aerosol spraying | 72 | 1800 at 1 C | 60 | 1500 after 120 cycles | 117 |
| Si NPs/G | Thermal reduction | 45 | 1143 at 0.3 A $g^{-1}$ | 63 | 800 after 30 cycles | 119 |
| Si NPs/G | Spray drying/thermal reduction | 80.9 | 1525 at 0.1 A $g^{-1}$ | 70 | 1500 at 0.2 A $g^{-1}$ after 30 cycles | 120 |
| Si NPs/G | Freeze drying/thermal reduction | 82.1 | 1866 at 0.2 A $g^{-1}$ | 60.8 | 1153 after 100 cycles | 122 |
| Si NPs/G | Microwave drying/ thermal reduction | 31 | 984 at 0.5 A $g^{-1}$ | 61 | 815 after 100 cycles | 124 |
| Si NPs/G | Freeze drying/thermal reduction | 65 | 1218 at 0.1 A $g^{-1}$ | 89.9 | 850 after 100 cycles | 128 |
| Si NPs/G | Freeze drying/thermal reduction | 91.7 | 1079 at 0.3 A $g^{-1}$ | 59.9 | 828 after 50 cycles | 131 |
| Si NPs/G | Freeze drying/thermal reduction | 80 | 2535 at 0.15 A $g^{-1}$ | 73.6 | 1984 after 40 cycles | 133 |
| Si NPs/G | Steam etching | 50 | 1536 at 0.05 A $g^{-1}$ | 48.8 | 1004 after 100 cycles | 125 |
| Si NPs/Ag | Chemical reduction using bulylamine | 97 | 1550 at 0.1 C | 80 | 1320 at 0.2 C after 100 cycles | 135 |
| Si NPs/Ag | Mechanical milling | 90 | 2050 at 0.1 mA $cm^{-2}$ | 83.4 | 800 after 30 cycles | 138 |
| Si NPs/PANi | *In-situ* polymerization | 75 | 1300 at 1.5 A $g^{-1}$ | 70 | 550 at 6.0 A $g^{-1}$ after 5000 cycles | 140 |
| Si NPs/PANi | *In-situ* polymerization | 87.7 | 2794 at 0.4 A $g^{-1}$ | 77.6 | 1546 after 50 cycles | 142 |
| Si NPs/PPy | Mechanical milling | 90 | 1919 at 0.126 A $g^{-1}$ | 53.4 | 100 after 40 cycles | 143 |

facilitating the formation of a stable SEI layer. Third, the conformal PANi coating surrounding each Si NP, as well as the conductive and continuous 3D framework, helps provide good electrical connection to the nanoparticles.

Table 2 presents a summary of the synthetic strategies and electrochemical characteristics of Si NPs-based composites reported in the literature recently. As described in Section 3 and listed in Table 2, the incorporation of conductive materials can effectively improve the electrochemical performance of Si NPs. It is interesting to combine the nanostructures such as solid nanostructures, hollow nanostructures and porous structures described in Section 2 with conductive material modification to enhance the performance of Si anodes.[148] For instance, Zhang *et al*.[149] prepared $SiO_x$ microparticles with homogeneously-embedded Si nanocrystals and nanopores *via* magnesiothermic reduction of $SiO_2$. The $SiO_x$ microparticles were further modified by PANi-Ag shell through *in-situ* polymerization. The obtained composite exhibited excellent cycling performance with a reversible capacity of 1149 mA h $g^{-1}$ after 100 cycles. The enhanced performance is mainly attributed to the combination of porous structure and high-electronic-conductivity PANi-Ag layers. Recently, porous Si was prepared in our group *via* the magnesiothermic reduction of MCM-41, followed by dual surface modification of Ag NPs and G.[150] The obtained composite showed a distinctly high reversible capacity, good cycling stability and super rate capability. An initial discharge capacity as high as 3531 mA h $g^{-1}$ was achieved at 0.1 A $g^{-1}$. A capacity of 1241 mA h $g^{-1}$ was still retained at a high current density of 32 A $g^{-1}$ for 50 cycles. The exceptional electrochemical performance of the composite is attributed to a synergistic effect, stemming from the combination of porous Si structure and dual surface modification. More recently, uniform porous Si hollow nanospheres (PHSi) were fabricated in our group through the magnesiothermic reduction of mesoporous $SiO_2$ hollow nanospheres ($MHSiO_2$). These hollow nanospheres were surface modified by subsequent *in-situ* chemical polymerization of PPy.[151] The as-prepared PPy@PHSi nanocomposite delivered a high initial discharge capacity of 2603 mA h $g^{-1}$ and showed an excellent cycling stability with 88% capacity retention against at the 2nd cycle after 250 cycles. SEM and TEM observations showed the spherical morphology and hollow structure of the nanocomposite are well maintained after cycling for 250 cycles (Fig. 13). Although volume expansion from 700 to over 900 nm is observed, no distinct fractures of Si and exfoliation of PPy coating are detected, indicating high structure stability of the nanocomposite. The combination of porous hollow Si structure and PPy coating can synergistically improve the electrochemical performance of the nanocomposite.

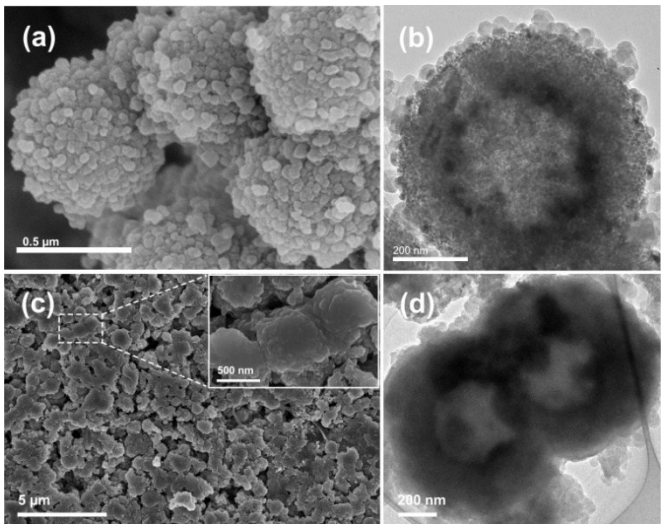


**Fig. 13** (a, b) SEM and TEM images of PPy@PHSi nanocomposite. (c) SEM image of PPy@PHSi nanocomposite on current collector after 250 cycles. (d) TEM image of PPy@PHSi nanocomposite after 250 cycles. Reprinted with permission from ref. 151. Copyright 2014 WILEY-VCH Verlag GmbH & Co. KGaA, Weinheim.

## 4. Other factors affecting performance

In addition to the structure, surface and interface impact, other factors such as electrolyte additives, binders, and current collectors also give significant influence on the capacity and cycle life of Si nanostructures and their composites.

### 4.1 Electrolyte additives

The SEI generated on the Si surface is usually unstable due to the formation of cracks caused by the large volume expansion of Si during the lithiation process. Fresh Si surfaces exposed would consume the electrolyte constantly, leading to the growth of a thick SEI layer, and ultimately poor electrochemical performance of the electrodes. In order to form a thin and stable SEI layer, chemicals including vinylene carbonate,[152-159] tris(pentafluorophenyl) borane,[160] succinic anhydride,[161,162] fluoroethylene carbonate (FEC)[157-159,163-166] have been added into the electrolytes to improve the performance of Si anodes. Particularly, FEC has been proved to be effective in enhancing the Coulombic efficiency and capacity retention of Si anodes. Utilizing FEC-containing electrolyte (FEC, 10 wt%), only 5% capacity (referring to 1200 mA h $g^{-1}$) was lost for Si NPs with particle size of ~50 nm and Coulombic efficiency of approximately 99% was retained after 80 cycles. In contrast, only 70% capacity was preserved without the addition of FEC and the Coulombic efficiency dropped to ~97% after 80 cycles.[163] It was also reported that the introduction of FEC into electrolyte (50 v/v%) increased the discharge capacity of Si thin film from approximately 2750 mA h $g^{-1}$ to above 3200 mA h $g^{-1}$, and also enhanced the Coulombic efficiency from about 98% to more than 99.5% after 30 cycles.[166] The improvement in the electrochemical performance of Si anodes by FEC additive is well investigated and attributed to the formation of stable FEC-derived SEI film.[163,164] The reduction products of FEC is mainly consist of –CHF-$OCO_2$ type compounds and LiF. These compounds form an initial SEI covered the Si surface evenly. This SEI film is mechanically strong enough to prevent the formation of large amounts of cracks, while the LiF contributes the $Li^+$ conductivity in the SEI film. In addition, the initially formed SEI

can alleviate the constant decomposition of electrolyte and thus prevent the continuous generation of a nonuniform SEI layer.

### 4.2 Binders

Polymers are usually employed to bind conducting particles and active materials together onto the current collector. The properties of binders play a critical role in the LIB performance, especially for the initial Coulombic efficiency and cycle stability. Poly(vinylidene fluoride) (PVDF) is commercially used as a binder in the fabrication of LIBs. However, it was found that the weak van der Waals interactions are not enough to sustain the electrode integrity during the huge volume change of Si between the fully lithiated and delithiated states.[167] Recently, considerable progress has been made in the exploit of functional binders that can enhance the integrity of Si electrode.[167-189] For instance, polymer binders containing carboxyl groups and their derivatives, such as polyacrylic acid (PAA),[168] carboxymethyl cellulose (CMC) based polymers,[169-171] and alginate (Alg) based polymers,[172-175] are employed as binders for Si materials. Compared with PVDF and styrene-butadiene rubber (SBR), these polymer binders show much high binding ability with Si, benefiting from the formation of hydrogen bonding and/or covalent chemical bonds. Recently, Kovalenko *et al*.[172] found that Si anode fabricated by using alginate as a binder showed better electrochemical performance than that by CMC. As shown in Fig. 14a, the reversible capacity of an Alg-based Si anode is over 1700 mA h $g^{-1}$ after 100 cycles at a current density of 4200 mA $g^{-1}$, while that of CMC-based Si is below 1000 mA h $g^{-1}$ after 40 cycles. In Alg, carboxyl groups are naturally present and evenly distributed in the polymer chain, whereas in MCM they are synthetically induced and their distribution is random. Multi-functional polymer binders have also been developed.[176,177] For example, Ryou *et al*.[176] conjugated adhesive catechol functional groups stemming from dopamine hydrochloride to PAA and Alg backbones. As shown in Fig. 14b and c, Si-Alg-C and Si-PAA-C showed better cycling stability than their counterparts without catechol groups. Although the introduction of such above-mentioned functional groups to the polymer chain exhibited higher adhesion associated with better performance of Si anode, the linear chain nature of these polymer binders is prone to sliding upon the continuous volume variation of Si during cycling. To address this issue, 3D polymer networks, in which the polymer chain was anchored by a cross-linking technique, were sequentially prepared for the Si anodes.[173-175,178-183] Koo *et al*.[178] reported a 3D cross-linked polymeric binder prepared by a condensation reaction of PAA and CMC. The c-PAA-CMC binder with Si NPs showed better cycling stability than CMC, PAA and PVDF (Fig. 14d). More recently, self-healing polymers (SHPs) containing abundant hydrogen bonds were used as binders to stabilize Si anodes.[184,185] SHPs have both mechanical and electrical healing

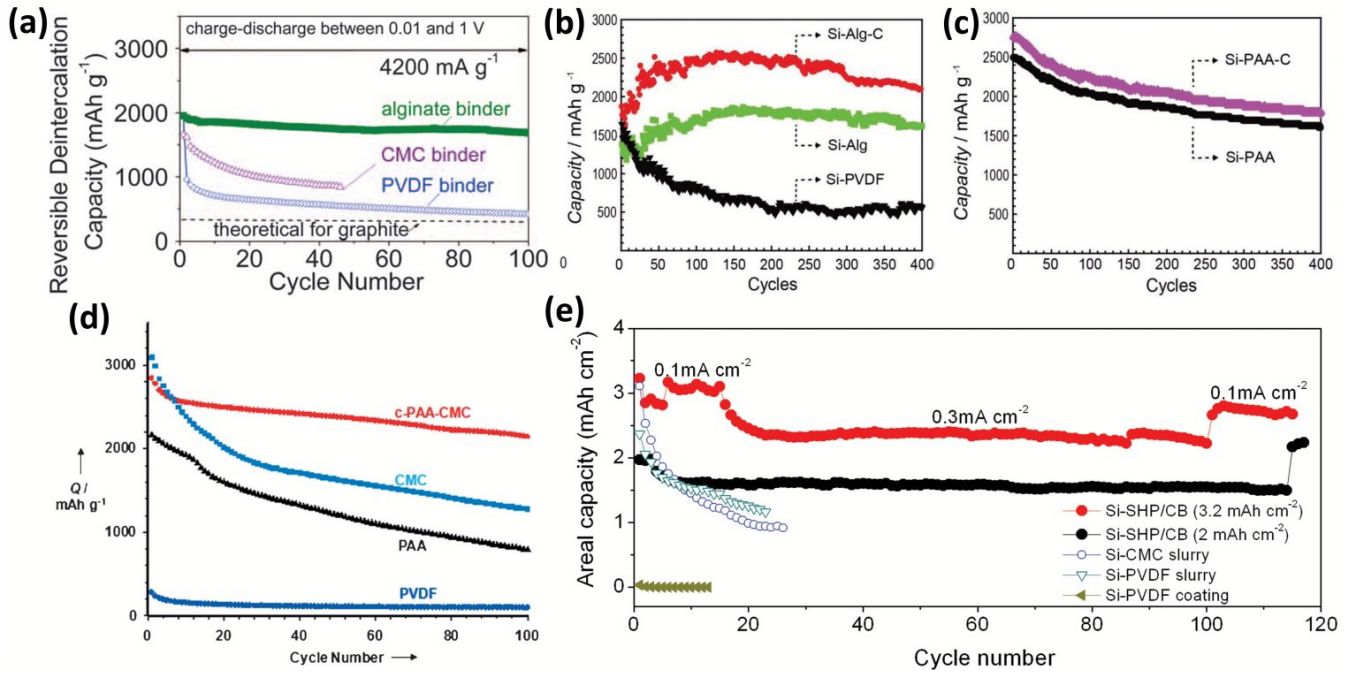


**Fig. 14** (a) The cycling performance of the Si NP electrodes with PVDF, CMC, and Alg binders measured at a current density of 4200 mA $g^{-1}$. Reprinted with permission from ref. 172. Copyright 2011 American Association for the Advancement of Science. (b, c) The cycling performance of the Si electrodes based on the Alg-C, Alg, PVDF, PAA-C, and PAA binders measured at a current density of 2100 mA $g^{-1}$. Reprinted with permission from ref. 176. Copyright 2013 WILEY-VCH Verlag GmbH & Co. KGaA, Weinheim. (d) The cycling performance of the Si electrodes employing the c-PAA-CMC, CMC, PAA, and PVDF binders measured at a current density of 300 mA $g^{-1}$. Reprinted with permission from ref. 178. Copyright 2012 WILEY-VCH Verlag GmbH & Co. KGaA, Weinheim. (e) The cycling performance of the Si-SHP/CB (1.13 $mg_{si}$ $cm^{-2}$), Si-SHP/CB (0.72 $mg_{si}$ $cm^{-2}$), Si-CMC slurry, Si-PVDF slurry, and Si-PVDF coating electrodes. Reprinted with permission from ref. 184. Copyright 2015 WILEY-VCH Verlag GmbH & Co. KGaA, Weinheim.

capabilities, allowing fractures and damages of Si to repeatedly heal during battery cycling. As shown in Fig. 14e, the Si-SHP/carbon black (Si-SHP/CB) electrode with a high mass loading of 1.13 $mg_{si}$ $cm^{-2}$ delivered an initial areal capacity of approximately 3.22 mA h $cm^{-2}$ at a current of 0.1 mA $cm^{-2}$, and maintained a high areal capacity of 2.72 mA h $cm^{-2}$ at a current of 0.3 mA $cm^{-2}$ after about 120 cycles. In comparison, Si electrodes with the same Si and similar mass loadings using CMC or PVDF as binder exhibited rapid capacity fade after a few cycles.[184]

### 4.3 Current collectors

Current collector, offering a good electrical connection between the active materials and the external circuit, is essential for high performance of the electrode. In order to improve the electrical contact between the active Si material and the current collector, porous or rough substrates were produced by sand-papering,[190-192] electrochemical etching[193-195] and electrodeposition.[195,196] Si-based thin film can firmly attach to such modified substrates, lowering electrical contact resistance and prolonging the cycle life of the electrodes. Recently, 3D porous metal foams are used to as negative current collectors for LIBs[197-200] Compared with traditional Cu foil, 3D porous metal foams have large specific surface areas, increasing mass loading of active materials and consequently the energy density of LIBs. Moreover, the open-porous framework of metal foams can provide a fast transport pathway for the electrolyte and $Li^+$, leading to a better rate performance. Si/RGO (RGO: reduced graphene oxide) nanostructures were coated onto a 3D porous Ni foam electrode by a dip-coating method (Fig. 15a).[197] This electrode showed exceptional good electrochemical performance, particularly in rate capability. The average discharge capacities were 2198, 2115, 1779, 1552, 975, and 700 mA h $g^{-1}$ at rates of 0.05, 0.1, 0.5, 1, 5, and 10 C, respectively. Moreover, the capacity retention of 87% could be achieved at a high rate of 10 C from cycle 48 to 200 (Fig. 15b). Mazouzi *et al*.[198] reported a Cu-foam/Si/C/CMC electrode prepared by loading the slurry of Si/C/CMC into the Cu foam by successive steps of impregnation. The electrode with an impressive Si loading of 10 mg $cm^{-2}$ exhibited a good cycleability more than 400 cycles when cycled with a limited capacity of 1200 mA h $g^{-1}$. More recently, non-metal current collectors, such as ultrathin-graphite foam (UGF),[201] CNF fabric,[99] G films[202,203] and CNT film,[204] were prepared and employed as current collectors for LIBs. The carbonaceous current collectors are lighter than metal current collectors, further improving the energy density of LIBs. For instance, Ji *et al*.[201] reported the preparation of a Si/G/UGF 3D electrode by drop-casting a composite of graphene-coated Si NPs on an UGF. The electrode has a 3D interconnected porous structure and the Si NPs are well dispersed on the UGF (Fig. 15c-e). Reversible capacities of 309 and 370 mA h $g^{-1}$ were achieved at a current density of 0.4 A $g^{-1}$ after 100 cycles for the electrodes with Si loading of 0.4 and 1.5 mg $cm^{-2}$, respectively (Fig. 15f), much higher than that of Si loaded on a metal foil.

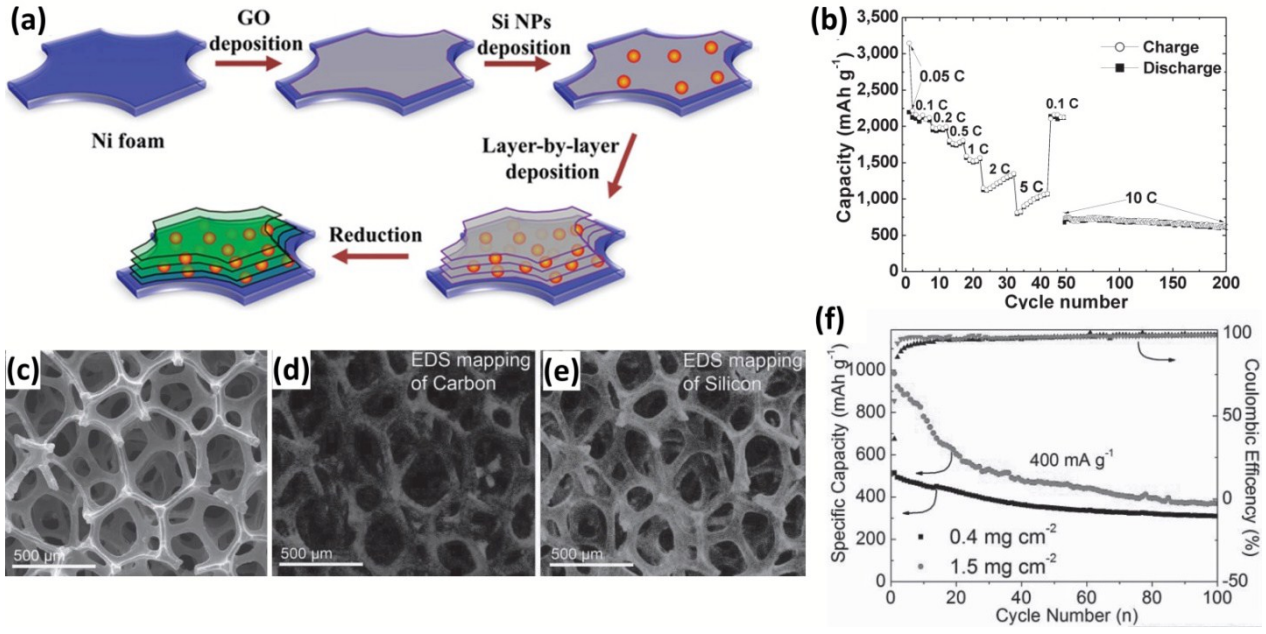


**Fig. 15** (a) Schematic preparation process for multilayered Si/RGO electrode. (b) Rate capability of the multilayered Si/RGO electrode at various current rates as marked. Reprinted with permission from ref. 197. Copyright 2013 WILEY-VCH Verlag GmbH & Co. KGaA, Weinheim. (c) SEM image of the structure of Si/G dropped on UGF. EDS element mapping images of (d) C and (e) Si acquired at the same region with Fig. c. (f) Cycling performance and coulombic efficiency of the Si/G/UGF electrodes at a current density of 0.4 A $g^{-1}$. Reprinted with permission from ref. 201. Copyright 2013 WILEY-VCH Verlag GmbH & Co. KGaA, Weinheim.

## 5. Summary and future perspective

Silicon with large gravimetric capacity and low lithium alloying potential has been regarded as one of the most promising anode materials for the development of LIBs with high energy densities and attracted considerable attention. However, silicon materials with low intrinsic electric and ionic conductivity suffer from large volume expansion during cycling, leading to rapid capacity decay. In the past decade, a variety strategies, such as structure and morphology control, surface and interface modification, electrolyte additive incorporation, novel polymer binder development, and appropriate current collector selection, have been developed and successfully improved the electrochemical performance of Si electrodes. Si nanostructures with controlled morphologies, such as thin films, nanosheets, nanorods, nanowires, nanotubes, hollow spheres, and hierarchically porous structures provide adequate void space to accommodate the huge volume change of Si during the lithiation and delithiation processes, enhancing the cycling stability. Moreover, these nanostructures facilitate electron transportation and $Li^+$ diffusion, improving the rate capability. However, most of the research is focused on the gravimetric capacities of Si nanostructured electrodes. Given the high porosity and large specific surface area, the volumetric capacities of Si nanostructures are usually not as promising as their gravimetric capacities. The volumetric energy density of LIBs is critical for some particular applications, such as portable electronics.

Si nanoparticles with controlled particle size have relatively high tap densities, and consequently ensure the volumetric energy density of LIBs. To suppress the volume variation and modify the physicochemical property of particle surface, many conductive species, including carbon coatings, carbon nanotubes and nanofibers, graphene nanosheets, metals, and conductive polymers, have been incorporated into Si nanoparticles to form a variety of composites. The introduction of conductive components to the Si nanoparticles can improve the electrical conductivity of the electrode, ensuring the high rate capability. The conductive components can alleviate the serious aggregation of Si nanoparticles, and suppress large volume expansion of Si nanoparticles upon alloying with lithium. The formation of surface coating would prevent the direct contact of Si nanoparticles with the electrolyte, ensuring the generation of stable SEI layer and consequently superior cycling stability. However, the content of the conductive components should be well controlled and optimized to achieve high volumetric energy density of LIBs.

The control of structure and morphology, and incorporation of conductive components during the material design and preparation process are effective strategies in improving the electrochemical performance of Si electrode. Parameters during the electrode and battery fabrication processes are also critical for the battery performance. The binders impact on the adhesion between current collectors and active materials and the integrity of the electrode upon cycling. Proper polymer binders and conductive additives involved in the electrode fabrication will decrease the inner resistance of the electrode, resulting in good rate and cycling performance. In addition, the addition of appropriate electrolyte additives can facilitate the formation of thin and stable SEI layer, contributing to the cycling stability. The morphology and surface property of current collectors should also be well designed to ensure the firm attachment of the electrode layers with the current collector and reduce the electrical contact resistance.

Although the above-mentioned approaches can improve the performance of Si anodes effectively, low-cost, reliable, and large-scale preparation of Si materials with controlled nanostructure and morphology is still challenging, impacting on their practical and commercial application as anodes in LIBs. Further work is required to understand and optimize the lithium ion transport kinetics within Si electrode and the interface between the electrode and electrolyte. In the consideration of full cell application, the gravimetric and volumetric capacities of Si electrodes and the content of conductive components during the formation of Si composites should be further optimized. Novel polymer binders and electrolyte additives should be developed. It is high desirable that the cross-linking of these polymers can also provide sufficient pathways for electrons. The research on Si electrode materials is a hot topic in the energy storage field. It is believed that with the fast development in this science and technology, the issues that hinder the practical application of Si electrodes will be well addressed and LIB with high energy density will be produced to meet the demand of stationary energy storage of renewable energy resources and electric vehicles.

## Acknowledgements

This work was financially supported by the National Basic Research Program of China (2013CB934102 and 2014CB932102) and the National Natural Science Foundation of China (21271128, 21331004, 51472158).

## Notes and references

1 K. X. Wang, X. H. Li and J. S. Chen, *Adv. Mater.*, 2015, **27**, 527-545.
2 P. Roy and S. K. Srivastava, *J. Mater. Chem. A*, 2015, **3**, 2454-2484.
3 X. L. Wu, Y. G. Guo and L. J. Wan, *Chem. Asian J.*, 2013, **8**, 1948-1958.
4 M. T. McDowell, S. W. Lee, W. D. Nix and Y. Cui, *Adv. Mater.*, 2013, **25**, 4966-4985.
5 M. R. Zamfir, H. T. Nguyen, E. Moyen, Y. H. Lee and D. Pribat, *J. Mater. Chem. A*, 2013, **1**, 9566-9586.
6 C. M. Park and H. J. Sohn, *Adv. Mater.*, 2007, **19**, 2465-2468.
7 L. Wang, X. He, J. Li, W. Sun, J. Gao, J. Guo and C. Jiang, *Angew. Chem., Int. Ed.*, 2012, **51**, 9034-9037.
8 Y. Wang, L. Tian, Z. Yao, F. Li, S. Li and S. Ye, *Electrochim. Acta*, 2015, **163**, 71-76.
9 H. Jia, R. Kloepsch, X. He, J. P. Badillo, P. Gao, O. Fromm, T. Placke and M. Winter, *Chem. Mater.*, 2014, **26**, 5683-5688.
10 D. J. Xue, S. Xin, Y. Yan, K. C. Jiang, Y. X. Yin, Y. G. Guo and L. J. Wan, *J. Am. Chem. Soc.*, 2012, **134**, 2512-2515.

11 F. H. Du, Y. S. Liu, J. Long, Q. C. Zhu, K. X. Wang, X. Wei and J. S. Chen, *Chem. Commun.*, 2014, **50**, 9961-9964.
12 J. Qin, C. He, N. Zhao, Z. Wang, C. Shi, E. Z. Liu and J. Li, *ACS Nano*, 2014, **8**, 1728-1738.
13 Z. Wen, S. Cui, H. Kim, S. Mao, K. Yu, G. Lu, H. Pu, O. Mao and J. Chen, *J. Mater. Chem.*, 2012, **22**, 3300-3306.
14 H. Hou, X. Tang, M. Guo, Y. Shi, P. Dou and X. Xu, *Mater. Lett.*, 2014, **128**, 408-411.
15 S. L. Chou, X. W. Gao, J. Z. Wang, D. Wexler, Z. X. Wang, L. Q. Chen and H. K. Liu, *Dalton Trans.*, 2011, **40**, 12801-12807.
16 G. Zhang, J. Zhu, W. Zeng, S. Hou, F. Gong, F. Li, C. C. Li and H. Duan, *Nano Energy*, 2014, **9**, 61-70.
17 H. Wu and Y. Cui, *Nano Today*, 2012, **7**, 414-429.
18 X. Su, Q. Wu, J. Li, X. Xiao, A. Lott, W. Lu, B. W. Sheldon and J. Wu, *Adv. Energy Mater.*, 2014, **4**, 1300882.
19 X. Chen, C. Li, M. Gratzel, R. Kostecki and S. S. Mao, *Chem. Soc. Rev.*, 2012, **41**, 7909-7937.
20 H. Jung, M. Park, S. H. Han, H. Lim and S. K. Joo, *Solid State Commun.*, 2003, **125**, 387-390.
21 H. Jung, M. Park, Y. G. Yoon, G. B. Kim, S. K. Joo, *J. Power Sources*, 2003, **115**, 346-351.
22 J. Graetz, C. C. Ahn, R. Yazami and B. Fultz, *Electrochem. Solid-State Lett.*, 2003, **6**, A194-A197.
23 G. Zhao, Y. Meng, N. Zhang and K. Sun, *Mater. Lett.*, 2012, **76**, 55-58.
24 H. Xia, S. Tang and L. Lu, *Mater. Res. Bull.*, 2007, **42**, 1301-1309.
25 C. Pereira-Nabais, J. Swiatowska, M. Rosso, F. Ozanam, A. Seyeux, A. Gohier, P. Tran-Van, M. Cassir and P. Marcus, *ACS Appl. Mater. Interfaces*, 2014, **6**, 13023-13033.
26 M. S. Park, G. X. Wang, H. K. Liu and S. X. Dou, *Electrochim. Acta*, 2006, **51**, 5246-5249.
27 L. B. Chen, J. Y. Xie, H. C. Yu and T. H. Wang, *J. Appl. Electrochem.*, 2009, **39**, 1157-1162.
28 T. Takamura, S. Ohara, M. Uehara, J. Suzuki and K. Sekine, *J. Power Sources*, 2004, **129**, 96-100.
29 J. Yin, M. Wada, K. Yamamoto, Y. Kitano, S. Tanase and T. Sakai, *J. Electrochem. Soc.*, 2006, **153**, A472-A477.
30 C. K. Chan, H. Peng, G. Liu, K. Mcllwrath, X. F. Zhang, R. A. Huggins and Y. Cui, *Nat. Nanotechnol.*, 2008, **3**, 31-35.
31 K. Peng, J. Jie, W. Zhang and S. T. Lee, *Appl. Phys. Lett.*, 2008, **93**, 033105.
32 P. P. Prosini, C. Cento, F. Alessandrini, P. Gislon, A. Mancini, A. Rufoloni, F. Rondino and A. Santoni, *Solid State Ionics*, 2014, **260**, 49-54.
33 K. Q. Peng, X. Wang, L. Li, Y. Hu and S. T. Lee, *Nano Today*, 2013, **8**, 75-97.
34 A. Gohier, B. Laïk, J. P. Pereira-Ramos, C. S. Cojocaru and P. Tran Van, *J. Power Sources*, 2012, **203**, 135-139.
35 Y. Xiao, D. Hao, H. Chen, Z. Gong and Y. Yang, *ACS Appl. Mater. Interfaces*, 2013, **5**, 1681-1687.
36 Z. Wen, Z. Zhang and G. Wang, *RSC Adv.*, 2014, **4**, 57430-57435.
37 A. M. Chockla, K. C. Klavetter, C. B. Mullins and B. A. Korgel, *Chem. Mater.*, 2012, **24**, 3738-3745.
38 Z. Wen, J. Stark, R. Saha, J. Parker and P. A. Kohl, *J. Phys. Chem. C*, 2013, **117**, 8604-8610.
39 H. T. Nguyen, F. Yao, M. R. Zamfir, C. Biswas, K. P. So, Y. H. Lee, S. M. Kim, S. N. Cha, J. M. Kim and D. Pribat, *Adv. Energy Mater.*, 2011, **1**, 1154-1161.
40 N. S. Hieu, J. C. Lim and J. K. Lee, *Microelectron. Eng.*, 2012, **89**, 138-140.
41 S. H. Nguyen, J. C. Lim and J. K. Lee, *Electrochim. Acta*, 2012, **74**, 53-58.
42 R. Teki, M. K. Datta, R. Krishnan, T. C. Parker, T. M. Lu, P. N. Kumta and N. Koratkar, *Small*, 2009, **5**, 2236-2242.
43 Y. Zhou, X. Jiang, L. Chen, J. Yue, H. Xu, J. Yang and Y. Qian, *Electrochim. Acta*, 2014, **127**, 252-258.
44 H. Ghassemi, M. Au, N. Chen, P. A. Heiden and R. S. Yassar, *ACS Nano*, 2011, **5**, 7805-7811.
45 S. Soleimani-Amiri, S. A. S. Tali, S. Azimi, Z. Sanaee and S. Mohajerzadeh, *Appl. Phys. Lett.*, 2014, **105**, 193903.
46 Z. Bao, M. R. Weatherspoon, S. Shian, Y. Cai, P. D. Graham, S. M. Allan, G. Ahmad, M. B. Dickerson, B. C. Church, Z. Kang, H. W. Abernathy III, C. J. Summers, M. Liu and K. H. Sandhage, *Nature*, 2007, **446**, 172-175.
47 Z. Lu, J. Zhu, D. Sim, W. Zhou, W. Shi, H. H. Hng and Q. Yan, *Chem. Mater.*, 2011, **23**, 5293-5295.
48 X. Yu, F. Xue, H. Huang, C. Liu, J. Yu, Y. Sun, X. Dong, G. Cao and Y. Jung, *Nanoscale*, 2014, **6**, 6860-6865.
49 M. H. Park, M. G. Kim, J. Joo, K. Kim, J. Kim, S. Ahn, Y. Cui and J. Cho, *Nano Lett.*, 2009, **9**, 3844-3847.
50 J. K. Yoo, J. Kim, Y. S. Jung and K. Kang, *Adv. Mater.*, 2012, **24**, 5452-5456.
51 H. Wu, G. Chan, J. W. Choi, I. Ryu, Y. Yao, M. T. McDowell, S. W. Lee, A. Jackson, Y. Yang, L. Hu and Y. Cui, *Nat. Nanotechnol.*, 2012, **7**, 310-315.
52 Y. Yao, M. T. McDowell, I. Ryu, H. Wu, N. Liu, L. Hu, W. D. Nix and Y. Cui, *Nano Lett.*, 2011, **11**, 2949-2954.
53 D. Chen, X. Mei, G. Ji, M. Lu, J. Xie, J. Lu and J. Y. Lee, *Angew. Chem., Int. Ed.*, 2012, 51, 2409-2413.
54 M. Ge, J. Rong, X. Fang, A. Zhang, Y. Lu and C. Zhou, *Nano Res.*, 2013, 6, 174-181.
55 B. M. Bang, J. I. Lee, H. Kim, J. Cho and S. Park, *Adv. Energy Mater.*, 2012, **2**, 878-883.
56 M. Ge, Y. Lu, P. Ercius, J. Rong, X. Fang, M. Mecklenburg and C. Zhou, *Nano Lett.*, 2014, **14**, 261-268.
57 A. Esmanski and G. A. Ozin, *Adv. Funct. Mater.*, 2009, **19**, 1999-2010.
58 H. Kim, B. Han, J. Choo and J. Cho, *Angew. Chem., Int. Ed.*, 2008, **47**, 10151-10154.
59 Y. Yu, L. Gu, C. Zhu, S. Tsukimoto, P. A. van Aken and J. Maier, *Adv. Mater.*, 2010, **22**, 2247-2250.
60 H. Jia, P. Gao, J. Yang, J. Wang, Y. Nuli and Z. Yang, *Adv. Energy Mater.*, 2011, **1**, 1036-1039.
61 P. Gao, H. Jia, J. Yang, Y. Nuli, J. Wang and J. Chen, *Phys. Chem. Chem. Phys.*, 2011, **13**, 20108-20111.
62 D. P. Wong, R. Suriyaprabha, R. Yuvakumar, V. Rajendran, Y. T. Chen, B. J. Hwang, L. C. Chen and K. H. Chen, *J. Mater. Chem. A*, 2014, **2**, 13437-13441.
63 N. Liu, K. Huo, M. T. McDowell, J. Zhao and Y. Cui, *Sci. Rep.*, 2013, **3**, 1919.
64 A. Xing, S. Tian, H. Tang, D. Losic and Z. Bao, *RSC Adv.*, 2013, **3**, 10145-10149.
65 M. S. Wang, L. Z. Fan, M. Huang, J. Li and X. Qu, *J. Power Sources*, 2012, **219**, 29-35.
66 L. Shen, X. Guo, X. Fang, Z. Wang and L. Chen, *J. Power Sources*, 2012, **213**, 229-232.
67 Y. Zhao, X. Liu, H. Li, T. Zhai and H. Zhou, *Chem. Commun.*, 2012, **48**, 5079-5081.
68 Y. Liu, B. Chen, F. Cao, H. L. W. Chan, X. Zhao and J. Yuan, *J. Mater. Chem.*, 2011, **21**, 17083-17086.
69 M. Ge, X. Fang, J. Rong and C. Zhou, *Nanotechnology*, 2013, **24**, 422001.
70 A. Magasinski, P. Dixon, B. Hertzberg, A. Kvit, J. Ayala and G. Yushin, *Nat. Mater.*, 2010, **9**, 353-358.
71 J. Yu, J. Yang, X. Feng, H. Jia, J. Wang and W. Lu, *Ind. Eng. Chem. Res.*, 2014, **53**, 12697-12704.
72 H. Tao, L. Z. Fan, W. L. Song, M. Wu, X. He and X. Qu, *Nanoscale*, 2014, **6**, 3138-3142.
73 N. Liu, Z. Lu, J. Zhao, M. T. McDowell, H. W. Lee, W. Zhao and Y. Cui, *Nat. Nanotechnol.*, 2014, **9**, 187-192.
74 M. S. Wang and L. Z. Fan, *J. Power Sources*, 2013, **244**, 570-574.

75 H. H. Li, J. W. Wang, X. L. Wu, H. Z. Sun, F. M. Yang, K. Wang, L. L. Zhang, C. Y. Fan and J. P. Zhang, *RSC Adv.*, 2014, **4**, 36218-36225.
76 Y. Park, N. S. Choi, S. Park, S. H. Woo, S. Sim, B. Y. Jang, S. M. Oh, S. Park, J. Cho and K. T. Lee, *Adv. Energy Mater.*, 2013, **3**, 206-212.
77 L. Pan, H. Wang, D. Gao, S. Chen, L. Tan and L. Li, *Chem. Commun.*, 2014, **50**, 5878-5880.
78 M. S. Wang, Y. Song, W. L. Song and L. Z. Fan, *ChemElectroChem*, 2014, **1**, 2124-2130.
79 J. Park, G. P. Kim, I. Nam, S. Park and J. Yi, *Nanotechnology*, 2013, **24**, 025602.
80 W. h. Lee, D. Y. Kang, J. S. Kim, J. K. Lee and J. H. Moon, *RSC Adv.*, 2015, **5**, 17424-17428.
81 X. Li, P. Meduri, X. Chen, W. Qi, M. H. Engelhard, W. Xu, F. Ding, J. Xiao, W. Wang, C. Wang, J. G. Zhang and J. Liu, *J. Mater. Chem.*, 2012, **22**, 11014-11017.
82 S. Chen, M. L. Gordin, R. Yi, G. Howlett, H. Sohn and D. Wang, *Phys. Chem. Chem. Phys.*, 2012, **14**, 12741-12745.
83 P. Gao, J. Fu, J. Yang, R. Lv, J. Wang, Y. Nuli and X. Tang, *Phys. Chem. Chem. Phys.*, 2009, **11**, 11101-11105.
84 R. D. Cakan, M. M. Titirici, M. Antonietti, G. Cui, J. Maier and Y. S. Hu, *Chem. Commun.*, 2008, 3759-3761.
85 J. Bae, *Colloid. Polym. Sci.*, 2011, **289**, 1233-1241.
86 S. H. Ng, J. Wang, D. Wexler, K. Konstantinov, Z. P. Guo and H. K. Liu, *Angew. Chem., Int. Ed.*, 2006, **45**, 6896-6899.
87 X. Y. Zhou, J. J. Tang, J. Yang, J. Xie and L. L. Ma, *Electrochim. Acta*, 2013, **87**, 663-668.
88 N. Liu, H. Wu, M. T. McDowell, Y. Yao, C. Wang and Y. Cui, *Nano Lett.*, 2012, **12**, 3315-3321.
89 L. Su, J. Xie, Y. Xu, L. Wang, Y. Wang and M. Ren, *Phys. Chem. Chem. Phys.*, 2015, **17**, 17562-17565.
90 L. Su, Z. Zhou and M. Ren, *Chem. Commun.*, 2010, **46**, 2590-2592.
91 T. H. Hwang, Y. M. Lee, B. S. Kong, J. S. Seo and J. W. Choi, *Nano Lett.*, 2012, **12**, 802-807.
92 X. Zhou, L. J. Wan and Y. G. Guo, *Small*, 2013, **9**, 2684-2688.
93 D. Nan, Z. H. Huang, R. Lv, Y. Lin, L. Yang, X. Yu, L. Ye, W. Shen, H. Sun and F. Kang, *J. Nanomater.*, 2014, 139639.
94 Y. Li, Z. Lin, G. Xu, Y. Yao, S. Zhang, O. Toprakci, M. Alcoutlabi and X. Zhang, *ECS Electrochem. Lett.*, 2012, **1**, A31-A33.
95 Z. L. Xu, B. Zhang, S. Abouali, M. A. Garakani, J. Huang, J. Q. Huang, E. K. Heidari and J. K. Kim, *J. Mater. Chem. A*, 2014, **2**, 17944-17951.
96 H. P. Liu, W. M. Qiao, L. Zhan and L. C. Ling, *New Carbon Mater.*, 2009, **24**, 124-130.
97 L. Ji and X. Zhang, *Electrochem. Commun.*, 2009, **11**, 1146-1149.
98 B. S. Lee, S. B. Son, K. M. Park, J. H. Seo, S. H. Lee, I. S. Choi, K. H. Oh and W. R. Yu, *J. Power Sources*, 2012, **206**, 267-273.
99 Y. Liu, K. Huang, Y. Fan, Q. Zhang, F. Sun, T. Gao, Z. Wang and J. Zhong, *Electrochim. Acta*, 2013, **102**, 246-251.
100 Y. Li, B. Guo, L. Ji, Z. Lin, G. Xu, Y. Liang, S. Zhang, O. Toprakci, Y. Hu, M. Alcoutlabi and X. Zhang, *Carbon*, 2013, **51**, 185-194.
101 L. Ji and X. Zhang, *Carbon*, 2009, **47**, 3219-3226.
102 W. Wang and P. N. Kumta, *ACS Nano*, 2010, **4**, 2233-2241.
103 C. Martin, O. Crosnier, R. Retoux, D. Belanger, D. M. Schleich and T. Brousse, *Adv. Funct. Mater.*, 2011, **21**, 3524-3530.
104 A. Gohier, B. Laik, K. H. Kim, J. L. Maurice, J. P. Pereira-Ramos, C. S. Cojocaru and P. T. Van, *Adv. Mater.*, 2012, **24**, 2592-2597.
105 Y. S. Na, S. Choi and D. W. Park, *Phys. Status Solidi A*, 2014, **211**, 2749-2755.
106 Y. Fan, Q. Zhang, Q. Xiao, X. Wang and K. Huang, *Carbon*, 2013, **59**, 264-269.
107 L. Yue, H. Zhong and L. Zhang, *Electrochim. Acta*, 2012, **76**, 326-332.
108 R. Epur, M. K. Datta and P. N. Kumta, *Electrochim. Acta*, 2012, **85**, 680-684.
109 Y. S. Na, H. Yoo, T. H. Kim, J. Choi, W. I. Lee, S. Choi and D. W. Park, *Thin Solid Films*, 2015, **587**, 14-19.
110 T. Cetinkaya, M. O. Guler and H. Akbulut, *Microelectron. Eng.*, 2013, **108**, 169-176.
111 W. J. Yu, C. Liu, P. X. Hou, L. Zhang, X. Y. Shan, F. Li and H. M. Cheng, *ACS Nano*, 2015, **9**, 5063-5071.
112 N. Coppey, L. Noe, M. Monthioux and B. Caussat, *Chem. Eng. Res. Des.*, 2013, **91**, 2491-2496.
113 B. G. Kim, W. H. Shin, S. Y. Lim, B. S. Kong and J. W. Choi, *J. Electrochem. Sci. Technol.*, 2012, **3**, 116-122.
114 V. Chabot, K. Feng, H. W. Park, F. M. Hassan, A. R. Elsayed, A. Yu, X. Xiao and Z. Chen, *Electrochim. Acta*, 2014, **130**, 127-134.
115 J. Zhang, L. Zhang, P. Xue, L. Zhang, X. Zhang, W. Hao, J. Tian, M. Shen and H. Zheng, *J. Mater. Chem. A*, 2015, **3**, 7810-7821.
116 J. G. Ren, Q. H. Wu, G. Hong, W. J. Zhang, H. Wu, K. Amine, J. Yang and S. T. Lee, *Energy Technol.*, 2013, **1**, 77-84.
117 Y. Wen, Y. Zhu, A. Langrock, A. Manivannan, S. H. Ehrman and C. Wang, *Small*, 2013, **9**, 2810-2816.
118 X. Zhou, Y. X. Yin, L. J. Wan and Y. G. Guo, *Adv. Energy Mater.*, 2012, **2**, 1086-1090.
119 H. Xiang, K. Zhang, G. Ji, J. Y. Lee, C. Zou, X. Chen and J. Wu, *Carbon*, 2011, **49**, 1787-1796.
120 Y. S. He, P. Gao, J. Chen, X. Yang, X. Z. Liao, J. Yang and Z. F. Ma, *RSC Adv.*, 2011, **1**, 958-960.
121 J. Luo, X. Zhao, J. Wu, H. D. Jang, H. H. Kung and J. Huang, *J. Phys. Chem. Lett.*, 2012, **3**, 1824-1829.
122 X. Zhou, Y. X. Yin, L. J. Wan and Y. G. Guo, *Chem. Commun.*, 2012, **48**, 2198-2200.
123 G. Zhao, L. Zhang, Y. Meng, N. Zhang and K. Sun, *J. Power Sources*, 2013, **240**, 212-218.
124 F. Maroni, R. Raccichini, A. Birrozzi, G. Carbonari, R. Tossici, F. Croce, R. Marassi and F. Nobili, *J. Power Sources*, 2014, **269**, 873-882.
125 H. Tang, J. Zhang, Y. J. Zhang, Q. Q. Xiong, Y. Y. Tong, Y. Li, X. L. Wang, C. D. Gu and J. P. Tu, *J. Power Sources*, 2015, **286**, 431-437.
126 S. L. Chou, J. Z. Wang, M. Choucair, H. K. Liu, J. A. Stride and S. X. Dou, *Electrochem. Commun.*, 2010, **12**, 303-306.
127 X. Zhao, C. M. Hayner, M. C. Kung and H. H. Kung, *Adv. Energy Mater.*, 2011, **1**, 1079-1084.
128 Y. Chen, X. Zhang, Y. Tian and X. Zhao, *J. Nanomater.*, 2014, 734751.
129 D. P. Wong, H. P. Tseng, Y. T. Chen, B. J. Hwang, L. C. Chen and K. H. Chen, *Carbon*, 2013, **63**, 397-403.
130 Y. S. Ye, X. L. Xie, J. Rick, F. C. Chang and B. J. Hwang, *J. Power Sources*, 2014, **247**, 991-998.
131 S. Yang, G. Li, Q. Zhu and Q. Pan, *J. Mater. Chem.*, 2012, **22**, 3420-3425.
132 N. Lin, J. Zhou, Y. Zhu and Y. Qian, *J. Mater. Chem. A*, 2014, **2**, 19604-19608.
133 B. Xu, H. Wu, C. X. Lin, B. Wang, Z. Zhang and X. S. Zhao, *RSC Adv.*, 2015, **5**, 30624-30630.
134 R. C. de Guzman, J. Yang, M. M. C. Cheng, S. O. Salley and K. Y. S. Ng, *J. Mater. Sci.*, 2013, **48**, 4823-4833.
135 S. Yoo, J. I. Lee, S. Ko and S. Park, *Nano Energy*, 2013, **2**, 1271-1278.
136 S. Murugesan, J. T. Harris, B. A. Korgel and K. J. Stevenson, *Chem. Mater.*, 2012, **24**, 1306-1315.
137 S. Yang and Q. Pan, *Electrochem. Solid-State Lett.*, 2011, **14**, A180-A184.

138 X. Yang, Z. Wen, S. Huang, X. Zhu and X. Zhang, *Solid State Ionics*, 2006, **177**, 2807-2810.
139 Z. P. Guo, J. Z. Wang, H. K. Liu and S. X. Dou, *J. Power Sources*, 2005, **146**, 448-451.
140 H. Wu, G. Yu, L. Pan, N. Liu, M. T. McDowell, Z. Bao and Y. Cui, *Nat. Commun.*, 2013, **4**, 1943.
141 M. Kummer, J. P. Badillo, A. Schmitz, H. G. Bremes, M. Winter, C. Schulz and H. Wiggers, *J. Electrochem. Soc.*, 2014, **161**, A40-A45.
142 M. Feng, J. Tian, H. Xie, Y. Kang and Z. Shan, *J. Solid State Electrochem.*, 2015, **19**, 1773-1782.
143 X. Y. Zhou, J. J. Tang, J. Yang, Y. L. Zou, S. C. Wang, J. Xie and L. L. Ma, *Electrochim. Acta*, 2012, **70**, 296-303.
144 S. Y. Chew, Z. P. Guo, J. Z. Wang, J. Chen, P. Munroe, S. H. Ng, L. Zhao and H. K. Liu, *Electrochem. Commun.*, 2007, **9**, 941-946.
145 H. S. La, K. S. Park, K. S. Nahm, K. K. Jeong and Y. S. Lee, *Colloids Surf., A*, 2006, **272**, 22-26.
146 H. C. Tao, X. L. Yang, L. L. Zhang and S. B. Ni, *J. Solid State Electrochem.*, 2014, **18**, 1989-1994.
147 M. Gu, X. C. Xiao, G. Liu, S. Thevuthasan, D. R. Baer, J. G. Zhang, J. Liu, N. D. Browning and C. M. Wang, *Sci. Rep.*, 2014, **4**, 3684.
148 L. Su, Y. Jing and Z. Zhou, *Nanoscale*, 2011, **3**, 3967-3983.
149 P. Zhang, L. Wang, J. Xie, L. Su and C. A. Ma, *J. Mater. Chem. A*, 2014, **2**, 3776-3782.
150 F. H. Du, K. X. Wang, W. Fu, P. F. Gao, J. F. Wang, J. Yang and J. S. Chen, *J. Mater. Chem. A*, 2013, 1, 13648-13654.
151 F. H. Du, B. Li, W. Fu, Y. J. Xiong, K. X. Wang and J. S. Chen, *Adv. Mater.*, 2014, **26**, 6145-6150.
152 M. Q. Li, M. Z. Qu, X. Y. He and Z. L. Yu, *Electrochim. Acta*, 2009, **54**, 4506-4513.
153 L. Chen, K. Wang, X. Xie and J. Xie, *J. Power Sources*, 2007, **174**, 538-543.
154 M. Ulldemolins, F. Le Cras, B. Pecquenard, V. P. Phan, L. Martin and H. Martinez, *J. Power Sources*, 2012, **206**, 245-252.
155 Y. Xiao, D. Hao, H. Chen, Z. Gong and Y. Yang, *ACS Appl. Mater. Interfaces*, 2013, **5**, 1681-1687.
156 L. Chen, K. Wang, X. Xie and J. Xie, *Electrochem. Solid-State Lett.*, 2006, **9**, A512-A515.
157 S. Dalavi, P. Guduru and B. L. Lucht, *J. Electrochem. Soc.*, 2012, **159**, A642-A646.
158 I. A. Profatilova, C. Stock, A. Schmitz, S. Passerini and M. Winter, *J. Power Sources*, 2013, **222**, 140-149.
159 C. C. Nguyen and B. L. Lucht, *J. Electrochem. Soc.*, 2014, **161**, A1933-A1938.
160 G. B. Han, J. N. Lee, J. W. Choi and J. K. Park, *Electrochim. Acta*, 2011, **56**, 8997-9003.
161 G. B. Han, M. H. Ryou, K. Y. Cho, Y. M. Lee and J. K. Park, *J. Power Sources*, 2010, **195**, 3709-3714.
162 Y. Li, G. Xu, Y. Yao, L. Xue, S. Zhang, Y. Lu, O. Toprakci and X. Zhang, *J. Solid State Electrochem.*, 2013, **17**, 1393-1399.
163 C. Xu, F. Lindgren, B. Philippe, M. Gorgoi, F. Bjorefors, K. Edstrom and T. Gustafsson, *Chem. Mater.*, 2015, **27**, 2591-2599.
164 X. Chen, X. Li, D. Mei, J. Feng, M. Y. Hu, J. Hu, M. Engelhard, J. Zheng, W. Xu, J. Xiao, J. Liu and J. G. Zhang, *ChemSusChem*, 2014, **7**, 549-554.
165 K. Leung, S. B. Rempe, M. E. Foster, Y. Ma, J. M. Martinez del la Hoz, N. Sai and P. B. Balbuena, *J. Electrochem. Soc.*, 2014, **161**, A213-A221.
166 H. Nakai, T. Kubota, A. Kita and A. Kawashima, *J. Electrochem. Soc.*, 2011, **158**, A798-A801.
167 Y. K. Jeong, T. W. Kwon, I. Lee, T. S. Kim, A. Coskun and J. W. Choi, *Energy Environ. Sci.*, 2015, **8**, 1224-1230.
168 A. Magasinski, B. Zdyrko, I. Kovalenko, B. Hertzberg, R. Burtovyy, C. F. Huebner, T. F. Fuller, I. Luzinov and G. Yushin, *ACS Appl. Mater. Interfaces*, 2010, **2**, 3004-3010.
169 B. Lestriez, S. Bahri, I. Sandu, L. Roue and D. Guyomard, *Electrochem. Commun.*, 2007, **9**, 2801-2806.
170 D. Shao, H. Zhong and L. Zhang, *ChemElectroChem*, 2014, **1**, 1679-1687.
171 J. Guo and C. Wang, *Chem. Commun.*, 2010, **46**, 1428-1430.
172 I. Kovalenko, B. Zdyrko, A. Magasinski, B. Hertzberg, Z. Milicev, R. Burtovyy, I. Luzinov and G. Yushin, *Science*, 2011, **334**, 75-79.
173 J. Liu, Q. Zhang, Z. Y. Wu, J. H. Wu, J. T. Li, L. Huang and S. G. Sun, *Chem. Commun.*, 2014, **50**, 6386-6389.
174 J. Yoon, D. X. Oh, C. Jo, J. Lee and D. S. Hwang, *Phys. Chem. Chem. Phys.*, 2014, **16**, 25628-25635.
175 L. Zhang, L. Zhang, L. Chai, P. Xue, W. Hao and H. Zheng, *J. Mater. Chem. A*, 2014, **2**, 19036-19045.
176 M. H. Ryou, J. Kim, I. Lee, S. Kim, Y. K. Jeong, S. Hong, J. H. Ryu, T. S. Kim, J. K. Park, H. Lee and J. W. Choi, *Adv. Mater.*, 2013, **25**, 1571-1576.
177 M. Wu, X. Xiao, N. Vukmirovic, S. Xun, P. K. Das, X. Song, P. Olalde-Velasco, D. Wang, A. Z. Weber, L. W. Wang, V. S. Battaglia, W. Yang and G. Liu, *J. Am. Chem. Soc.*, 2013, **135**, 12048-12056.
178 B. Koo, H. Kim, Y. Cho, K. T. Lee, N. S. Choi and J. Cho, *Angew. Chem., Int. Ed.*, 2012, **51**, 8762-8767.
179 J. Song, M. Zhou, R. Yi, T. Xu, M. L. Gordin, D. Tang, Z. Yu, M. Regula and D. Wang, *Adv. Funct. Mater.*, 2014, **24**, 5904-5910.
180 L. Shen, L. Shen, Z. Wang and L. Chen, *ChemSusChem*, 2014, **7**, 1951-1956.
181 Y. Park, S. Lee, S. H. Kim, B. Y. Jang, J. S. Kim, S. M. Oh, J. Y. Kim, N. S. Choi, K. T. Lee and B. S. Kim, *RSC Adv.*, 2013, **3**, 12625-12630.
182 Z. J. Han, N. Yabuuchi, S. Hashimoto, T. Sasaki and S. Komaba, *ECS Electrochem. Lett.*, 2013, **2**, A17-A20.
183 T. Yim, S. J. Choi, J. H. Park, W. Cho, Y. N. Jo, T. H. Kim and Y. J. Kim, *Phys. Chem. Chem. Phys.*, 2015, **17**, 2388-2393.
184 Z. Chen, C. Wang, J. Lopez, Z. Lu, Y. Cui and Z. Bao, *Adv. Energy Mater.*, 2015, **5**, 1401826.
185 C. Wang, H. Wu, Z. Chen, M. T. McDowell, Y. Cui and Z. Bao, *Nat. Chem.*, 2013, **5**, 1042-1048.
186 L. Yue, L. Zhang and H. Zhong, *J. Power Sources*, 2014, **247**, 327-331.
187 T. W. Kwon, Y. K. Jeong, I. Lee, T. S. Kim, J. W. Choi and A. Coskun, *Adv. Mater.*, 2014, **26**, 7979-7985.
188 S. J. Park, H. Zhao, G. Ai, C. Wang, X. Song, N. Yuca, V. S. Battaglia, W. Yang and G. Liu, *J. Am. Chem. Soc.*, 2015, **137**, 2565-2571.
189 M. Ling, Y. Xu, H. Zhao, X. Gu, J. Qiu, S. Li, M. Wu, X. Song, C. Yan, G. Liu and S. Zhang, *Nano Energy*, 2015, **12**, 178-185.
190 Y. E. Roginskaya, T. L. Kulova, A. M. Skundin, M. A. Bruk, E. N. Zhikharev and V. A. Kal'nov, *Russ. J. Electrochem.*, 2008, **44**, 992-1001.
191 H. Guo, H. Zhao, C. Yin and W. Qiu, *Mater. Sci. Eng., B*, 2006, **131**, 173-176.
192 K. L. Lee, J. Y. Jung, S. W. Lee, H. S. Moon and J. W. Park, *J. Power Sources*, 2004, **129**, 270-274.
193 T. Takamura, M. Uehara, J. Suzuki, K. Sekine and K. Tamura, *J. Power Sources*, 2006, **158**, 1401-1404.
194 C. C. Nguyen and S. W. Song, *Electrochim. Acta*, 2010, **55**, 3026-3033.
195 D. Reyter, S. Rousselot, D. Mazouzi, M. Gauthier, P. Moreau, B. Lestriez, D. Guyomard and L. Roue, *J. Power Sources*, 2013, **239**, 308-314.
196 T. Zhang, H. P. Zhang, L. C. Yang, B. Wang, Y. P. Wu and T. Takamura, *Electrochim. Acta*, 2008, **53**, 5660-5664.

197 J. Chang, X. Huang, G. Zhou, S. Cui, P. B. Hallac, J. Jiang, P. T. Hurley and J. Chen, *Adv. Mater.*, 2014, **26**, 758-764.
198 D. Mazouzi, D. Reyter, M. Gauthier, P. Moreau, D. Guyomard, L. Roue and B. Lestriez, *Adv. Energy Mater.*, 2014, **4**, 1301718.
199 C. Gao, H. Zhao, P. Lv, T. Zhang, Q. Xia and J. Wang, *ACS Appl. Mater. Interfaces*, 2015, **7**, 1693-1698.
200 X. Huang, H. Yu, J. Chen, Z. Lu, R. Yazami and H. H. Hng, *Adv. Mater.*, 2014, **26**, 1296-1303.
201 J. Ji, H. Ji, L. L. Zhang, X. Zhao, X. Bai, X. Fan, F. Zhang and R. S. Ruoff, *Adv. Mater.*, 2013, **25**, 4673-4677.
202 J. Z. Wang, C. Zhong, S. L. Chou and H. K. Liu, *Electrochem. Commun.*, 2010, **12**, 1467-1470.
203 H. C. Tao, L. Z. Fan, Y. Mei and X. Qu, *Electrochem. Commun.*, 2011, **13**, 1332-1335.
204 S. L. Chou, Y. Zhao, J. Z. Wang, Z. X. Chen, H. K. Liu and S. X. Dou, *J. Phys. Chem. C*, 2010, **114**, 15862-15867.